#### **PAPER**

# Method for electromechanical modeling of Johnson noise in Advanced LIGO

To cite this article: Edgard Bonilla et al 2021 Class. Quantum Grav. 38 025014

View the article online for updates and enhancements.



## IOP ebooks™

Bringing together innovative digital publishing with leading authors from the global scientific community.

Start exploring the collection-download the first chapter of every title for free.

https://doi.org/10.1088/1361-6382/abc571

### Method for electromechanical modeling of Johnson noise in Advanced LIGO

### Edgard Bonilla<sup>1,\*</sup>, Pablo Giuliani<sup>2</sup>, Brian Lantz<sup>1</sup> and Aaron Buikema<sup>3</sup>

- <sup>1</sup> Stanford University, Stanford, CA 94305, United States of America
- <sup>2</sup> Florida State University, Tallahassee, FL 32306, United States of America
- <sup>3</sup> LIGO, Massachusetts Institute of Technology, Cambridge, MA 02139, United States of America

E-mail: edgard@stanford.edu

Received 23 July 2020, revised 14 October 2020 Accepted for publication 28 October 2020 Published 14 December 2020



#### **Abstract**

We develop a complete framework for modeling general electromechanical systems in the quasi-electrostatic regime. The equations are applicable to a broad range of electrostatic problems and offer the advantage of being theoretically tractable for scaling arguments. Additionally, we show how the formalism can be used together with finite element simulations to obtain estimates for non-stationary effects such as charge accumulation in insulators. As a demonstration, we combined the formalism with measurements from Advanced LIGO to give an updated estimate for the Johnson noise coupling to the gravitational-wave channel. The induced signal was determined to be 10 times lower than the instrument's design sensitivity in the detection band and scaling as  $f^{-2}$ .

Keywords: Johnson noise, LIGO, Electromechanics

(Some figures may appear in colour only in the online journal)

#### 1. Introduction

The first direct detection of gravitational waves (GW) [1] confirmed the predictions derived from Einstein's general theory of relativity more than a century ago. This first detection of a black hole–black hole merger in 2015 has been followed by more than 50 more detection candidates [2, 3], including first observation of GW produced by a neutron star—neutron star merger [4]. This single event opened a new window in our understanding of the Universe

<sup>\*</sup>Author to whom any correspondence should be addressed.

through multimessenger astronomy: in this case the observation of both GW and electromagnetic radiation. The continuous improvement of the detectors' signal-to-noise ratio is casting new light on astrophysical questions such as the Hubble constant  $H_0$  [5], the equation of state in neutron stars [6], the mass-gap and population distributions of BBHs [7]. By the end of the third observation run, the detection of candidate GW signals was occurring more than once per week [8].

Continued reduction in the noise floor of the detectors is a high priority for the field. The design specifications for the detector noise are typically given by the noise from quantum mechanics of the optical system and thermal noise of the optical coatings and suspensions, and are often called the 'fundamental noise' for a particular design. However, at the low-frequency end of the detection band, i.e. from 10 Hz to around 50–70 Hz, the actual performance is typically limited by so-called 'technical noise' [9, 10]. Some of the noise sources, such as coupling from the angular control system, have been identified but there remains some for which the source is not well understood. At the end of O3a, this 'technical noise' was responsible for a significant reduction of the astrophysical reach of the LIGO Livingston Observatory (LLO), cutting the volume of observable space in half [11].

Careful analysis of possible noise sources is therefore a high priority. Noise from charge has long been a source of concern. The test masses are insulators, they are affected by spatially inhomogeneous and temporally varying charge accumulations [12], and are driven by electrostatic actuators [10]. A variety of calculations for several expected noise sources have been done, but these all make important simplifying assumptions [13, 14].

In this paper, we aim to lay the theoretical groundwork for a systematic study of the sources of technical noise that have an electromechanical origin, as well as illustrating the framework's applications. Section 2 lays out the assumptions and equations for modeling a general electromechanical system in the quasi-electrostatic regime. The section concludes by introducing what we call the electromechanical reciprocity relation, which constitutes the central relationship that enables us to perform all of the calculations and inferences that this article presents. In sections 3 and 5, we apply part of the theory to show that the Johnson noise of the electrostatic actuators is not large enough to impact Advanced LIGO's sensitivity, regardless of the timevarying charge accumulation observed around the test masses. Additionally, in section 4 we show that by pre-calculating the geometric potentials for the configuration (with finite element modeling), it is then straightforward to carry that solution to the estimation of the effect of arbitrary free charge distributions on the actuation strength. In future studies, we plan to use these simulations, together with the insight from the theoretical framework, to obtain the likelihood of particular charge accumulations given the variations in the actuation strength measured at the observatories.

Interested readers can also refer to appendices B and C to learn more about the implications of the electromechanic reciprocity relations and how to leverage them for different electromechanical calculations. Appendix A contains a set of simple examples to help digest the more abstract results of the paper, while also serving to provide insight into how the framework can deal with the different elements of a complex electromechanical environment. Finally, appendix D provides the full general derivation for the electromechanical equations. These equations can be used as the starting point for more accurate electromechanical models for current or future gravitational-wave observatories.

#### 2. Theoretical framework

#### 2.1. Problem statement

We frame the problem in the context of linear electrostatics theory by assuming: (a) magnetic effects can be neglected<sup>4</sup>, (b) the surface of every conductor remains a well-defined equipotential at all times, and (c) all the circuits and dielectrics involved have linear responses to driven voltage perturbations. Assumption (a) is justified by the fact that the velocities of all objects in our system are very small compared to the speed of light. Assumption (b) is justified by the small resistivity of the various metals in the vicinity of the Advanced LIGO test masses, which provides very small relaxation times, keeping the surfaces of the conductor as equipotentials for the frequencies of interest<sup>5</sup>. In regard of assumption (c) the fused silica test mass, its coatings and other non-conductors in the array behave like linear dielectrics<sup>6,7</sup>. The related circuits are linear in the frequencies of interest, which we conclude from parsing the various schematics shown in [21].

Under these assumptions, our system consists of an electrical and a mechanical part, an illustrative example shown in figure 1. The electrical part is composed of conductors  $(\mathcal{C})$ , dielectrics  $(\mathcal{D})$  and possible free charges  $(\rho_{\text{free}})$ . The mechanical part is a subset of the electrical components, comprised of objects  $(\mathcal{O})$  like the test mass, on which both mechanical and electrical forces can act. The objects move rigidly in both position and orientation, but they cannot be deformed.

For the remainder of this article, we will consider the rigid body translation of a single mechanical object  $\mathcal{O}$ , representing one of the Advanced LIGO test masses. The general case, including rotations and multiple moving objects is detailed in appendix D, but the general conclusions derived in this section remain the same.

The conductors of the system are connected through linear circuits to voltage sources with fixed potentials  $\phi^{\rm in}$ . The actual potential  $\phi_i$  on the surface of each conductor  $\mathcal{C}_i$  will depend on their fixed potential  $\phi_i^{\rm in}$ , the potential on the surfaces on the other conductors  $\phi_j$ , the positions of the dielectrics and free charges and finally the position  $\vec{r}$  of the object  $\mathcal{O}$ . In turn, the position of the object will depend on both the mechanical and electrical forces acting on it, the latter one sensitive to the potential at the surface of each conductor.

The potential at the surface of each conductor  $\phi_i$  and the position of each one of the mechanical objects  $\vec{r}$  describe the state of the system<sup>8</sup>. Since the Jonhson noise is small we are interested in the limit of small oscillations. We assume that the object's position and conductors' potentials oscillate around their equilibrium values by a small quantity:  $\delta \vec{r}$  and  $\delta \phi_i$  respectively.

Under this assumption and taking the  $\delta \vec{r}$  and  $\delta \phi_i$  as our variables, the electromechanical problem can be separated into two coupled systems, one electrical and one mechanical. We show in the next sections that after the small oscillations approximation is made, the electric

<sup>&</sup>lt;sup>4</sup> We work under the quasistatic approximation:  $\nabla \times E \approx 0$ . Which means that the electric field can be written as the gradient of a scalar potential. This approximation is justified when the length and time scales of our system satisfy  $\frac{L}{2} \ll c$  [15]. The spatial scale of our system is  $L \sim 1$  m, and the shortest time scale of interest is of order  $\tau \sim 10^{-3}$  s.

<sup>&</sup>lt;sup>5</sup> For a conductor the relaxation time can be defined as  $\rho\epsilon_0$  [16], where  $\rho$  is the resistivity and  $\epsilon_0$  the vacuum permittivity. The resistivity of the various metals surrounding the advanced LIGO test masses satisfy  $\rho\lesssim 10^{-6}$  Ωm. Since we are interested in frequencies below 10 kHz, then the relation  $\rho\epsilon_0\ll 1/f_{\rm max}$  is satisfied.

<sup>&</sup>lt;sup>6</sup> The mass coatings are layers of silica and titania-doped tantala [17], the earthquake stops are rubber with silica tips [18], and the ring heater is made of metals and glass [19].

<sup>&</sup>lt;sup>7</sup> One proposed upgrade to the observatories suggests using silicon test masses [20]. Since silicon is a semiconductor, a more detailed analysis will be required to account for the effect of nonlinearities in the Johnson noise estimates.

<sup>&</sup>lt;sup>8</sup> Alternatively, we could replace one or more of the conductor potentials  $\phi_i$  by their total charge  $q_i$  as the generalized coordinate. This description is analogous to the one presented in this article.

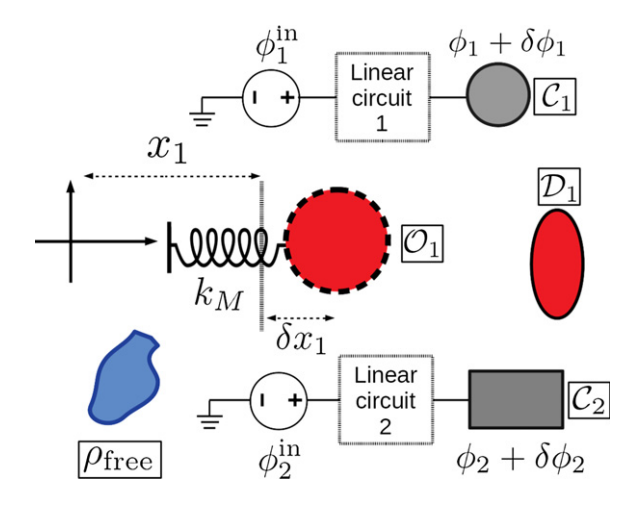


Figure 1. (a) Simplified example of the electromechanic system. The set of conductors  $\mathcal C$  shown in gray are connected to voltage sources with potentials  $\phi^{\rm in}$  through linear circuits. The potential  $\phi_i$  at the surface of each conductor  $\mathcal C_i$  is shifted by a small amount  $\delta\phi_i$ . The dielectrics  $\mathcal D_j$  are shown in red and the free charge  $\rho_{\rm free}$  is shown in blue. The mechanical object  $\mathcal O_k$ , a dielectric, is shown in red with dashed boundaries. The object is mechanically bounded by a force modeled by a spring. The equilibrium position of the objects measured from the coordinates origin  $x_k$  is shifted by a small amount  $\delta x_k$ .

system is transformed into a circuit for the variables  $\delta \phi_i$  with external input currents that depend on the coordinates of the object  $\delta r_k$ . In a similar way, the mechanical system can be simplified to a set of objects in harmonic potentials around their equilibrium positions, together with forces linear on the potentials  $\delta \phi_i$ .

#### 2.2. Circuit equations

In order to write the circuit equations we first note that the linear circuits that connect the conductors  $C_i$  to their respective voltage sources  $\phi_i^{\text{in}}$  can be replaced by their Thévenin equivalents [22] <sup>9</sup>.

This immediately implies that in equilibrium, we expect the potentials  $\phi_i = \phi_i^{\text{Th}}$ . Small oscillations  $\delta \phi_i$  around this equilibrium will result in currents through the impedances. Charge conservation implies that any current going through each subcircuit has to equal time derivative of the charge of the conductors, consequently:<sup>10</sup>

$$\frac{1}{Z_i^{\text{eq}}} \delta \phi_i = -\frac{d}{dt} \delta q_i = -\left[ \sum_j \left( \frac{\partial q_i}{\partial \phi_j} \right)_0 \frac{d\delta \phi_j}{dt} + \sum_k \left( \frac{\partial q_i}{\partial r_k} \right)_0 \frac{d\delta r_k}{dt} \right], \tag{1}$$

where the left-hand side is just the impedance version of Ohm's law and we expanded the perturbed charges  $\delta q_i$  in terms of the independent variables of the system. The zero subscript represents evaluation in the equilibrium position and potentials. We identify the derivatives  $\left(\frac{\partial q_i}{\partial \phi_j}\right)_0$  in equation (1) to be the coefficients of capacitance  $(\mathbf{C_0})_{ij}$  [16, 23] of the system of

<sup>&</sup>lt;sup>9</sup> i.e. each circuit is replaced by a single complex impedance  $Z_i^{\text{eq}}$  connected to an ideal potential source  $\phi_i^{\text{Th}}$ .

<sup>&</sup>lt;sup>10</sup> We use the notation Z<sup>eq</sup> very loosely in equation (2) for the sake of clarity. However, the complex impedance picture is only valid in frequency space, so we need to apply Fourier transforms before drawing any quantitative conclusions.

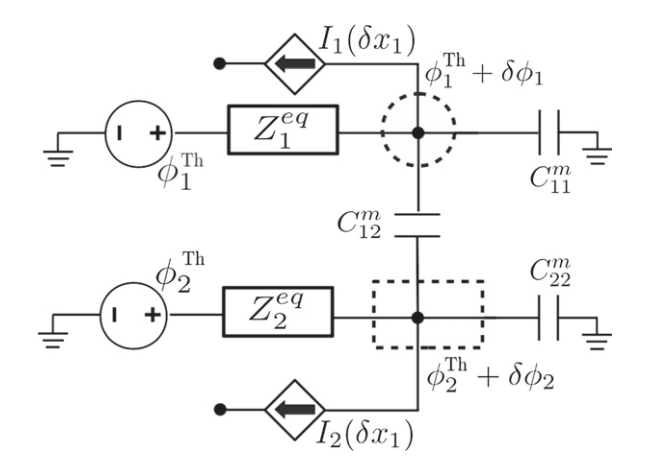


Figure 2. Electrical part of the simplified instance shown in figure 1. After the Thévenin relationships are applied, the linear circuits connected to the source potentials  $\phi_i^{\text{in}}$  are replaced by equivalent potentials  $\phi_i^{\text{Th}}$  and an effective complex impedance  $Z_i^{\text{eq}}$ . The interactions between the different conductors are replaced by effective mutual capacitances  $\mathbf{C}^{\text{m}}$  that include the effect of dielectrics and free charges. Each conductor's  $\mathcal{C}_i$  interaction with the motion of the object  $\mathcal{O}$  is replaced by one dependent current generator  $I_i$ , representing an internal rearrangement of charges. The current generators, the effective capacitors and the potential sources all connect through a conductor node, displayed as a black dot inside a dotted boundary. The circuit potential at these nodes correspond to the actual potential in the surface of the conductors.

conductors and dielectrics at equilibrium. The capacitance mediates the interaction between the potentials  $\delta\phi_i$  that describe the electrical part of the system.

The second sum in equation (1) acts like an extra current term  $I_i$  that is dependent on the mechanical variables  $\delta r_k$  of the system. It is mediated by the coefficients  $\left(\frac{\partial q_i}{\partial r_k}\right)_0$  which we will explore later, as they play an important role in the Johnson noise estimation.

With the introduction of the capacitance matrix  $C_0$ , equation (1) can be represented as a circuit diagram, where we replace the effect of the interaction between the conductors and dielectrics by a mutual capacitance network  $C^m$  [24], and we include branches with dependent current sources for the interaction with the mechanical system, as depicted in figure 2.

It is important to note that, although the excess potentials  $\delta\phi_i$  in the conductor nodes of figure 2 are exactly the same as the excess potential on the actual conductors  $\mathcal{C}_i$  (shown in figure 1), the excess charges are not. This can be inferred by noting that the dependent currents  $I_i$  represent the charge redistribution *inside* the conductors  $\mathcal{C}_i$ , necessary to keep them as equipotentials as the mechanical variables are perturbed. The charges associated with the conductor nodes in figure 2 are the ones associated with the potential perturbations  $\delta\phi_i$ .

Having defined the capacitance matrix we can write the equations that describe the electric part of the system as:

$$(\mathbf{Z}^{\text{eq}})^{-1}\delta\vec{\phi} + \mathbf{C}_{\mathbf{0}}\delta\dot{\vec{\phi}} + \left(\frac{\partial\vec{\mathbf{q}}}{\partial\vec{\mathbf{r}}}\right)_{0}\delta\dot{\vec{r}} = 0,$$
(2)

where the overhead dot represents time differentiation,  $\vec{q} = [q_1, \dots, q_N]$  and  $\delta \vec{\phi} = [\delta \phi_1, \dots, \delta \phi_N]$  are the instantaneous total charges and perturbed potentials of the conductors, respectively.  $(\mathbf{Z}^{\text{eq}})^{-1}$  is a diagonal matrix that represents the inverse of the equivalent impedances of each subcircuit, and we introduced the Jacobian  $\left(\frac{\partial \vec{q}}{\partial \vec{r}}\right)_{ik} = \frac{\partial q_i}{\partial r_k}$ . These equations contain the relations between the variables of the system  $\delta \phi_i$  and  $\delta r_k$  and will be coupled to the mechanical equations that we develop in the next subsection.

#### 2.3. Mechanical equations

In this subsection we derive the mechanical equations that govern the movement of the object  $\mathcal{O}$ . At the equilibrium positions and potentials, the total forces on the object  $\mathcal{O}$  are zero by definition. Small perturbations  $\delta \vec{r}$  and  $\delta \phi_i$  around this equilibrium will generate a fluctuating force  $\delta \vec{F}$  on  $\mathcal{O}$ . Under the effect of this force, Newton's second law can be written as:

$$\mathbf{M}\ddot{\delta}\ddot{r} = \delta\vec{F} = \sum_{k} \left(\frac{\partial \vec{F}}{\partial r_{k}}\right)_{0} \delta r_{k} + \sum_{i} \left(\frac{\partial \vec{F}}{\partial \phi_{i}}\right)_{0} \delta \phi_{i},\tag{3}$$

where **M** is a diagonal matrix with the total mass m of the object  $\mathcal{O}$  in each diagonal entry.

We can associate the terms of equation (3) that are proportional to the mechanical variables  $\delta r_k$  to the opposite of a effective stiffness matrix  $\mathbf{K}_{\text{eff}}$  that relates the displacements of the object with the forces on it that bring it back into equilibrium. This is roughly equivalent to connecting the mobile object with a set of linear springs.

On the other hand, the second sum involves the perturbed force that depends on the conductor potentials  $\delta\phi_i$ . The coefficients  $\left(\frac{\partial\vec{F}}{\partial\phi_i}\right)_0$  that mediate the electromechanical interaction are crucial in the Johnson noise estimate and will be studied in section 3. If we denote them as the matrix elements of the Jacobian  $\frac{\partial\vec{F}}{\partial\vec{\Phi}}$ , we can write equation (3) as:

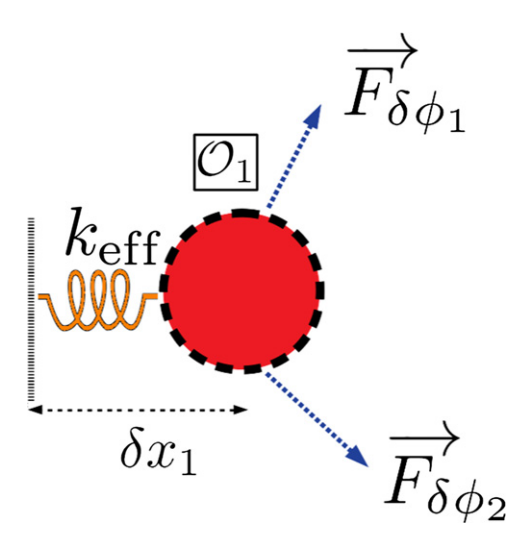
$$\mathbf{M}\ddot{\vec{\delta}}\vec{r} + \mathbf{K}_{\text{eff}}\delta\vec{r} - \left(\frac{\partial \vec{\mathbf{F}}}{\partial \vec{\Phi}}\right)_{0}\delta\vec{\phi} = 0.$$
 (4)

Figure 3 shows a free body diagram representing the mechanical and electrical components acting on the mobile object of figure 1. The electromechanical forces that depend on the position of the object have been abstracted to a single stiffness  $k_{\rm eff}^{\rm m}$ , and the interaction with the fluctuating potentials is shown as set of forces that depend on  $\delta\phi_i$ .

#### 2.4. Electromechanical reciprocity

Before proceeding with the Johnson noise estimates, we will briefly discuss an important relation between the two sets of *electromechanical coefficients*  $\frac{\partial q_i}{\partial r_k}$  and  $\frac{\partial F_k}{\partial \phi_i}$  that connect the electrical and mechanical variables in equations (2) and (4). These coefficients are not independent, in fact they are related through what we call the *electromechanical reciprocity relation*:

$$\frac{\partial q_i}{\partial r_k} = \frac{\partial F_k}{\partial \phi_i} \quad \Rightarrow \quad \frac{\partial \vec{\mathbf{q}}}{\partial \vec{\mathbf{r}}} = \left[ \frac{\partial \vec{\mathbf{F}}}{\partial \vec{\Phi}} \right]^{\mathrm{T}}.$$
 (5)



**Figure 3.** Mechanical part of the simplified instance shown in figure 1. Under the small oscillation approximation, the forces linear with the displacement  $\delta x_1$  are abstracted as an effective spring constant  $k_{\rm eff}$  attached to the equilibrium position. The interaction with the fluctuating potentials is shown as forces dependent on  $\delta \phi_i$ .

This equation is a consequence of the relation of the different variables and forces to the free energy available to the system in its electrostatic equilibrium states<sup>11</sup>. The rigorous proof for this equation and similar ones is given in the appendix.

It is important to highlight that the partial derivative  $\frac{\partial q_i}{\partial r_k}$  is performed by keeping the potentials  $\vec{\phi}$  constant while the partial derivative  $\frac{\partial F_k}{\partial \phi_i}$  is taken by keeping the position of the object  $\vec{r}$  constant. This follows from our choice of  $\delta \phi_i$  and  $\delta r_k$  as the independent variables of our system when performing the Taylor expansion in equations (1) and (3).

As a side note, let us suppose we want to actively control the position  $r_k$  of  $\mathcal O$  by applying a slowly changing potential  $\Delta\phi_i^{\rm in}$ , in a similar fashion to what is done with the electrostatic drive in Advanced LIGO [18]. This translates through the Thévenin equivalence to a fluctuation  $\Delta\phi_i^{\rm Th}$  in the potentials of the conductors. Then the applied force on  $\mathcal O$  is proportional to  $\frac{\partial F_k}{\partial \phi_i}\Delta\phi_i^{\rm Th}$ . Thus, the right-hand side of equation (5) represents the susceptibility of the mechanical system to electrostatic actuation.

On the other hand,  $\frac{\partial q_i}{\partial r_k} \delta \dot{r}_k$  represents the current that needs to be drawn to conductor i to keep the system at its equilibrium potentials ( $\delta \phi_i = 0, \forall i$ ) when  $\mathcal{O}$  is only moving in the  $r_k$  direction.

The conclusion from equation (5) is that the more sensitive the mechanical system is to the control forces coming from its electrical counterpart, the more backreaction current its motion will create in the circuits connected to the conductors. The current will pass through the impedances  $Z_i^{\text{eq}}$ , generating Joule heating in their dissipative elements. This energy loss mechanism is ultimately connected to the injection of thermal noise in the motion of  $\mathcal{O}$ .

<sup>&</sup>lt;sup>11</sup> This is similar to the Maxwell relations in thermodynamics [25]. The electrostatic assumptions of our formulation match the quasi-static ones oftentimes used to describe thermodynamic systems.

#### 3. Johnson noise calculation

Having derived the sets of coupled electromechanical equations together with the electromechanical reciprocity relation we proceed to estimate the fluctuations that the Johnson noise, generated in the electronic part of the circuit, produces on the position of the object  $\delta \vec{r}$ . These fluctuations are intimately related to the behavior of the dissipative parts of the electromechanical system, as described by the fluctuation–dissipation theorem [26, 27].

There are two equivalent approaches to this problem, and both yield the same result. The first one consists of modeling each of the N noisy impedances  $Z_i^{\rm eq}$  as a noiseless ideal impedance, connected in series with one of N independent white noise current sources  $\eta_i(t)$  with power spectral density given by  $|\hat{\eta}_i(f)|^2 = 4k_{\rm B}T~{\rm Re}[(Z_i^{\rm eq})^{-1}]$  [28]. Once the  $\eta_i$  are introduced, all that is left is to transform the equations onto the frequency space and solve for the noise forces they introduce in the mechanical object.

Alternatively, we can abstract the electrical part of the system by writing  $\delta \vec{\phi}$  as a function of the positions in equation (2) and substitute it into the mechanical equation (4). This is equivalent to treating the system as a position only problem, with a frequency-dependent viscous damping. Applying the fluctuation–dissipation theorem as outlined in [29] will yield the same result for the Johnson noise coupling.

To illustrate this calculation, consider the case of a single mobile object, representing the test mass moving in a single dimension. For the electrical part of the problem, assume we can describe the system with a single potential  $\phi$ . Finally, let the impedance of the circuit be a single resistance R. Under these assumptions, the electromechanical equations (2) and (4) simplify to:

$$m\ddot{\delta x} + k_{\text{eff}}\delta x - \left(\frac{\partial F_x}{\partial \phi}\right)_0 \delta \phi = 0,$$
 (6)

$$\frac{1}{R}\delta\phi + C_0\delta\dot{\phi} + \left(\frac{\partial q}{\partial x}\right)_0\delta\dot{x} = \eta(t). \tag{7}$$

We transform these equations into Fourier space and apply the electromechanical reciprocity to obtain:

$$\left(k_{\text{eff}} - m(2\pi f)^2\right)\delta\hat{x} - \left(\frac{\partial F_x}{\partial \phi}\right)_0 \delta\hat{\phi} = 0,\tag{8}$$

$$\left(\frac{1}{R} + i2\pi f C_0\right)\delta\hat{\phi} + i2\pi f \left(\frac{\partial F_x}{\partial \phi}\right)_0 \delta\hat{x} = \hat{\eta}(f). \tag{9}$$

We can now decouple these two equations and finally obtain the effective noise force on the object:

$$|F_{\eta}(f)| = \sqrt{4k_{\rm b}T} \left| \frac{\partial F_x}{\partial \phi} \right|_0 \sqrt{\frac{R}{1 + (2\pi fRC_0)^2}}.$$
 (10)

 $<sup>^{12}</sup>$  This is valid for the case of a single conductor with the potential at infinity set to zero, and for closed two-conductor arrays. Only one capacitance coefficient is necessary to describe these systems. The general case is left for the appendices.

If our frequencies of interest f are much bigger than the resonant frequencies of the electromechanical system (roughly meaning  $k_{\rm eff}/m \ll f^2$ ) then the object can be considered inertial and we obtain the frequency spectrum of  $\delta x$  as:

$$|\delta x_{\eta}(f)| \approx \frac{1}{m(2\pi f)^2} \sqrt{4k_b T} \left| \frac{\partial F_x}{\partial \phi} \right|_0 \sqrt{\frac{R}{1 + (2\pi f R C_0)^2}}.$$
 (11)

Even though equation (10) was derived for a simple system consisting of only one potential and one object constrained to move in a single dimension, we can highlight three important characteristic features that we expect to observe on the Johnson noise in more complex systems.

First, the noise amplitude is directly proportional to the actuation strength of the conductor  $\left(\frac{\partial F_x}{\partial \phi}\right)_0$ . Moreover, since  $\left(\frac{\partial F_x}{\partial \phi}\right)_0 = \left(\frac{\partial q}{\partial x}\right)_0$ , we see that the noise amplitude is proportional to the amount of current that gets generated from movements of the object. Since the current in the resistor is the source of damping, we see the electromechanical reciprocity is consistent with usual statement of the fluctuation–dissipation theorem [27].

Second, we can see that in the limiting cases  $R \to 0$  and  $R \to \infty$  the noise amplitude  $|x_{\eta}(f)| \to 0$ . In this simple example we can interpret  $R \to 0$  as a perfect connection between the conductor and its potential source, and  $R \to \infty$  as the conductor being completely disconnected from the circuits.

Third, above the resonant frequencies of the system, but given  $f \ll 1/RC_0$ , the displacement noise's spectral amplitude decays as  $1/f^2$ , which is the typical attenuation for force noises due to the inertia of  $\mathcal{O}$ . However, for higher frequencies ( $f \gg 1/RC_0$ ) the Johnson noise gets further attenuated by the latency on the charge and discharge time  $\tau = 1/RC_0$  of the circuit, falling off as  $1/f^3$  as a result. At these high frequencies, the capacitance acts as a low pass filter for any current noise coming from the circuit.

Returning to the more general case with one movable object and several conductors, if the charge and discharge time of the capacitor array is dominated by  $\mathbf{Z}^{eq}$  rather than  $\mathbf{C}_0$ , the noise's amplitude spectral density above the resonances of the system is given by:

$$|\delta x_{\eta}(f)| \approx \frac{\sqrt{4k_{\rm b}T}}{m(2\pi f)^2} \sqrt{\sum_{i\in\mathcal{C}} \left(\frac{\partial F_x}{\partial \phi_i}\right)_0^2 \operatorname{Re}(Z_i^{\rm eq})}.$$
 (12)

Here *x* is any of the mechanical variables describing the translation of an object with mass *m*. We expect this last limit to be valid for the electrostatic array used to control the Advanced LIGO test masses, since current-limiting capacitors have been set in all of the circuits [21] and the test mass can be considered inertial at the frequencies of interest. In section 5 we apply this result directly to estimate the Johnson noise coupling to the Advanced LIGO optic.

It is important to note, that under these assumptions, the estimation of the Jonhson noise relies on the value of the individual circuit's impedances  $Z_i^{\text{eq}}$  and the estimation of the electromechanical coefficients  $\left(\frac{\partial F_x}{\partial \phi_i}\right)_0$ .

#### 4. Extracting the electromechanical coefficients

The electromechanical coefficients are one of the main ingredients needed to estimate the Johnson noise spectral amplitude by using equation (12).

Thanks to the reciprocity relation (5) knowing either of the two sets of coefficients,  $\frac{\partial \vec{q}}{\partial \vec{r}}$  or  $\frac{\partial \vec{F}}{\partial \vec{q}}$ , is enough to estimate the Johnson noise amplitude in the system. Under that scope both

sets are equivalent, but since they are constructed from different concepts, each one presents its shortcuts and challenges at the time of estimation.

First, the coefficients  $\frac{\partial \vec{F}}{\partial \vec{\Phi}}$  are very easily measured if we consider their connection to electrostatic actuation. For a given electromechanic array, they can be obtained by individually driving the potentials  $\phi_i^{\text{in}}$  around their equilibrium values. From the electromechanical equation (2) and (3), we can find that the response on a coordinate x of the object  $\mathcal{O}$ , under the assumption that  $\mathbf{C}_0$  does not dominate the charge and discharge of the conductors  $\mathbf{C}_0$ , and above the mechanical resonances is related to the drive signal  $\Delta \phi_i^{\text{in}}$  by:

$$\left| \frac{\partial F_x}{\partial \phi_i} \right|_0 = m(2\pi f)^2 \left| \frac{\Delta x(f)}{\Delta \phi_i^{\text{in}}} \right| \left| \frac{\Delta \phi_i^{\text{in}}}{\Delta \phi_i^{\text{Th}}} \right|. \tag{13}$$

We recognize the first fraction of equation (13) as the transfer function between the input potentials and the motion  $\Delta x$  and the second one as the Thévenin relation for the input and the equivalent potential sources. The first one can be easily measured by driving the circuits and observing the response of the mechanical object at a frequency above the resonances. The second one can be inferred directly from the circuit schematics. This is the approach taken on section 5 when making the estimates for Advanced LIGO.

Direct modelling of  $\frac{\partial \vec{k}}{\partial \vec{\Phi}}$  for complex electrostatic environments can become challenging if free charges are present in the array. In principle, it requires not only knowing the free charge distribution beforehand but also a way to estimate the effect that the free charges have in the mechanical objects, which in turn reflects on the actuation strength of the conductors. Through this lens, even invoking the superposition principle, we need to run as many simulations as different densities  $\rho_{\rm free}$  we would like to evaluate.

On the other hand, the sets  $\frac{\partial \vec{q}}{\partial \vec{r}}$  would be difficult to measure experimentally, since one should be able to measure precisely how much charge is entering or leaving the conductor i when the object is moved a small amount  $dr_k$ . However, careful analysis reveals there is a shortcut to obtaining them by a computational simulation approach such as finite element modelling. The theoretical basis of how this can be done are left for appendix C, and the particular application to the study of the charge buildup around the Advanced LIGO test masses is left for a future manuscript. We show here a brief overview of the idea:

In the appendix C we show that the induced charge <sup>14</sup> in conductor *i* due to the presence of any free charge density  $\rho_{\text{free}}(\vec{r})$  can be calculated as:

$$(q_{\text{imag}})_i = -\int \rho_{\text{free}}(\vec{r}) f_i(\vec{r}) d^3 \vec{r}, \tag{14}$$

where we define  $f_i = \frac{\phi_i'(\vec{r})}{V_0}$ . The potential  $\phi_i'(\vec{r})$  is obtained by setting all the conductors to a reference potential (to be used as ground)<sup>15</sup> except for the *i*th one, which is set to  $V_0$ , in the absence of any free charge distribution  $\rho_{\text{free}}$ . Then, the function  $f_i$  represents a *geometric* potential at point  $\vec{r}$  and it is the proportionality between a free charge located at that point and the charge it induces on conductor i.

<sup>&</sup>lt;sup>13</sup> In the case of Advanced LIGO, the 10 nF current-limiting capacitor for the bias electrode circuit (shown in figure 4) is a good upper bound for the capacitance of the array. In the 10–100 Hz band, where measurements are made, we can consider that the array charges instantaneously.

<sup>&</sup>lt;sup>14</sup> The notation for equation (14) hints at the fact that we could think of this charge as the net 'image charge' induced on the conductors by the presence of free charge density.

<sup>&</sup>lt;sup>15</sup> In the case of Advanced LIGO, a very reasonable choice is the potential of the vacuum wall that surrounds the array.

To obtain the total charge in the conductors we just need to add  $\mathbf{C}_0\vec{\phi}$  to equation (14). Therefore, to obtain the coefficients  $\frac{\partial \vec{\mathbf{q}}}{\partial \vec{\mathbf{r}}}$  it is sufficient to know the geometric potentials  $f_i$ , the capacitance matrix  $\mathbf{C}_0$  and how they change due to a small displacement of the object. In a system with N conductors, for each degree of freedom, the finite differences can be computed in 2N simulations using a standard simulation package. The main advantage of this approach is that we could then use the superposition principle to calculate the effect of any charge distribution  $\rho_{\text{free}}$  on the electromechanic coefficients without having to simulate them explicitly.

#### 5. Johnson noise estimate for advanced LIGO

The Advanced LIGO tests masses are actuated directly via the electrostatic drives (ESDs). The drives consist of five different conducting bodies, one 'bias' electrode and four 'signal' electrodes [30]. By applying a DC bias on the bias electrode a polarization is induced on the test mass. The four signal electrodes are then used to apply forces on these polarized charges and thus actuate the test mass.

In principle, to properly estimate the Johnson noise contribution to the displacement noise of the test masses (and consequently to the gravitational-wave channel), it should be sufficient to measure the electromechanical coefficients  $\left(\frac{\partial F_y}{\partial \phi_i}\right)_0$  for each of the electrode voltages  $\phi_i$ . While there are such measurements available, the values for the actuation strength are sensitive to charge accumulation in the test mass' environment [30] and hence vary over time.

In consequence, we decided to provide a range for the estimate by using all the recent history of measurements for the actuation strength of the ESDs, recorded over the course of the third observing run at the LLO [31, 32].

The data for these measurements is given in terms of the coefficients that enter the semiempirical longitudinal force equation for the ESDs<sup>16</sup> [33]:

$$F = \alpha (V_{b} - V_{s})^{2} + \beta (V_{b} + V_{s}) + \beta_{2} (V_{b} - V_{s}) + \gamma (V_{b} + V_{s})^{2} + \delta, \tag{15}$$

where  $V_b$  and  $V_s$  are the potentials of the 'bias' and 'signal' electrodes. The assumption is made that all four signal electrodes are driven in unison.

Given this equation for the force, the electromechanical coefficients that participate in the Johnson noise equation (12) can be expressed as:

$$\left(\frac{\partial F}{\partial V_{b}}\right)_{0} = 2(\gamma + \alpha)V_{b}^{DC} + 2(\gamma - \alpha)V_{s}^{DC} + (\beta + \beta_{2}),$$

$$\left(\frac{\partial F}{\partial V_{s}}\right)_{0} = 2(\gamma - \alpha)V_{b}^{DC} + 2(\gamma + \alpha)V_{s}^{DC} + (\beta - \beta_{2}).$$
(16)

For the purposes of the Johnson noise estimates, we add the assumption that each signal electrode contributes one fourth of the actuation strength, before adding their contributions in quadrature. This is a reasonable assumption, given the measurements taken from the masses [31, 32].

 $<sup>^{16}</sup>$  In this equation, the potential of the cage surrounding the test mass is used as the reference. It is important to note that equation (15) contains all the information about the electrostatic environment surrounding the test masses. In particular, the coefficients  $\beta$  and  $\beta_2$  vary depending on free charge accumulation for the system. These facts are discussed briefly in appendix C, where we arrive at a version of this semi-empirical equation from first-principle electrostatics.

**Table 1.** Range for ESD force coefficients and nominal operating voltages measured at the LIGO Livingston Observatory during the third observing run. Extracted from [31, 32]. The columns correspond to each one of the two ETMs. Small differences in geometry and variations in the charge accumulation on the test masses and their surroundings account for the difference in the coefficients' values. The ranges for the coefficients (represented inside brackets) correspond to maximum and minimum values over the recorded data and are larger than the uncertainty associated with any individual measurement.

Parameters	Units	ETMX	ETMY
$\frac{(\gamma - \alpha)}{(\gamma + \alpha)}$	$10^{-10} \left( \text{N V}^{-2} \right) $ $10^{-10} \left( \text{N V}^{-2} \right)$	$\{-3.0; -1.0\}$ $\{3.2; 4.6\}$	$\{-4.0; -0.2\}$ $\{4.0; 5.4\}$
$(\beta - \beta_2)$	$10^{-8} (N V^{-1})$	$\{-0.3; 1.8\}$	$\{-5.6; 4.0\}$
$(\beta + \beta_2)$ $V_{\rm b}^{ m DC}$	$10^{-8} (N V^{-1})$ (V)	$\{-5.5; -0.3\}$ 350	$\{-7.6; -0.8\}$ 380
$V_{ m s}^{ m DC}$	(V)	0	0

**Table 2.** Estimated range for the electromechanical coefficients for the bias and the four signal electrodes (driven in unison) at the LIGO Livingston Observatory. The values displayed are the ranges for the absolute values obtained by using the coefficients from table 1 and equation (16). Note that for our estimates, the electromechanical coefficient for each one of the four signal electrode will be taken to be one quarter of the value presented in this table.

Units	ETMX	ETMY
$10^{-7} \left( \text{N V}^{-1} \right)$ $10^{-7} \left( \text{N V}^{-1} \right)$	{1.7; 3.2} {0.5: 2.1}	{2.3; 4.0} {0.0; 3.6}
		$10^{-7} (N V^{-1})$ {1.7; 3.2}

Of the four test masses at the LLO, only the two end test-masses (ETMs) are actively biased for actuation<sup>17</sup>. Hence they are the ones that will contribute in any significant way to the total Johnson noise coupling to the gravitational-wave channel<sup>18</sup>.

Table 1 shows a summary of the ranges for the measured parameters that are needed to calculate the electromechanical coefficients via equation (16). Table 2 shows the expected range for the absolute value of the electromechanical coefficients, which is in the range of  $10^{-7}$  N V<sup>-1</sup> for the bias electrodes. Note that for the signal electrodes the time-varying charging of the masses can have a substantial impact on the actuation strength.

The only missing piece to estimate the Johnson noise-induced displacement ASD of each test mass are the circuits connected to each electrode. The circuit diagrams shown in figure 4 were taken from [21] and correspond to the usual circuit paths for electrostatic actuation. The voltage outputs controlled by amplifiers are treated as ideal voltage sources and only elements after them are taken into consideration for our calculations.

To finish the Johnson noise estimate, we plug together the equivalent impedances from the circuits in figure 4 and the electromechanical coefficients from table 2 into equation (12),

 $<sup>^{\</sup>rm 17}\,\rm No$  control signals are sent to the ITMs during regular operation.

<sup>&</sup>lt;sup>18</sup> The input test-masses (ITMs) have  $V_b^{\rm DC} = V_s^{\rm DC} = 0$  V during operation. Moreover, the gap between ITMs and their respective ESDs is larger (20 mm) than the ETMs' (5 mm) [34] which drops the order of magnitude of their coefficients even lower [35].

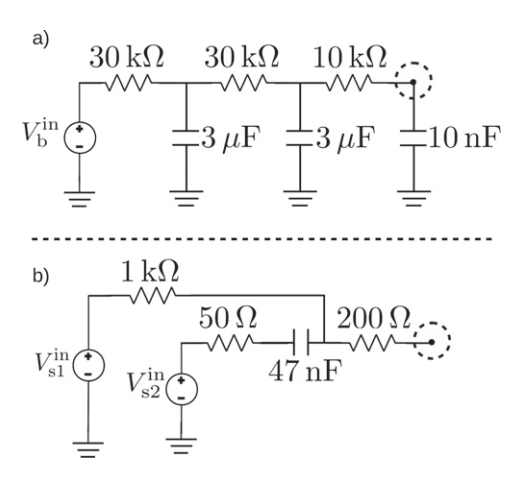
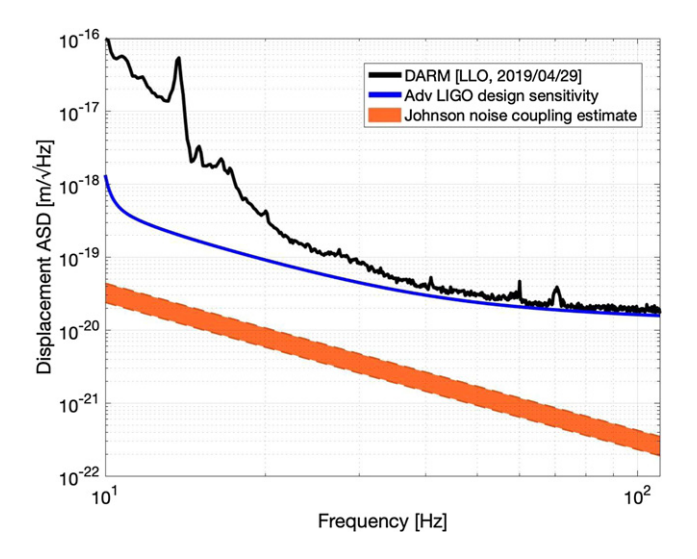


Figure 4. Schematics for the ESD circuits, extracted from [21]. (a) Bias path circuit, the final 10 nF capacitor suppresses the Johnson noise coupling at very high frequencies. The 3  $\mu$ F capacitors suppress noise at frequencies above  $\approx$  10 Hz. In the LIGO detection band the effective resistance is just the 10 k $\Omega$  resistor. (b) Circuit for each of the signal electrodes. Note that the overall impedance of this path, coupled with the overall smaller couplings imply that most of the Johnson noise contribution to the displacement noise comes from the bias circuit. The reason for using four signal electrodes, as well as two different voltage drives has to do with the active damping of the parametric instability of the cavity [36].



**Figure 5.** Estimate for the Johnson noise coupling to the gravitational-wave channel using the coefficients from [33, 35]. The estimated noise is 10 times lower than the instrument's design sensitivity at 20 Hz and falls as  $1/f^2$ . The sensitivity curves were created using the data from [37, 38].

for the two 40 kg ETMs. The result is shown in figure 5, where we can see that the contribution to the noise budget is about 10 times below the design sensitivity, sitting just under

 $5 \times 10^{-20}$  m Hz<sup>-0.5</sup> at 10 Hz and falling off as  $1/f^2$ . Most of the expected noise coupling comes from the unfiltered 10 k $\Omega$  resistor in the bias circuit.

It is important to note that the range of the time variation of the actuation strength does not appear to be large enough to make the Johnson noise coupling a dominant source of noise for the interferometer and thus it is an unlikely explanation for the unexplained sources of technical noise of the apparatus.

To give a sense of the scale of these results, we can compare the more rigorous estimate with a similar calculation made in [13], where the mass and drive are modelled as a parallel plate capacitor (this model is worked as an example of the more general framework in appendix A). Under this approximation, the results shown in figure 5 can be replicated if the two biased masses had effective capacitances of about 5 pF.  $^{19}$ 

A similar comparison can be drawn by assimilating the ESD to a circular conductive plate and the test mass to a point charge located in the axis of symmetry. As we shown in the appendix A.1, under this toy model a total unscreened net charge of 1.3  $\mu$ C in any of the test masses would cause the Johnson noise to hit the design sensitivity and become a relevant source of noise.

#### 6. Conclusions and future work

We presented a complete framework for modeling general electromechanical systems in the quasi-electrostatic regime. The formalism allows us to paint an accurate picture of the interaction of the circuits with the mechanical objects in terms of the electromechanic coefficients.

We show that this framework can be used to improve upon the preexisting estimates and models for the Advanced LIGO test mass—ESD array. Moreover, it can be used to understand some of the more complex interactions like the effect of charge accumulation on the actuation strength of the ESDs. In the future, we expect to be able to use a model of the geometric potentials together with the measurements of the actuation strength to help diagnose the charge buildup observed in the interferometers.

Additionally, we use the general framework to derive a set of qualitative conclusions about the electrostatic environment of the LIGO interferometers. We find that free charges in the system change the actuation strength even if not directly placed on the test masses and that the magnitude of Johnson noise coupling is intimately related to the charge and discharge time of the circuits. These points are fleshed out in appendix A.

Finally, as an example, we applied the framework to the estimation of the Johnson noise coupling to the gravitational-wave channel of the LLO, yielding a displacement noise just under  $5 \times 10^{-20}$  m Hz<sup>-0.5</sup> at 10 Hz and falling off as  $1/f^2$ . Since this value is about 10 times below the design sensitivity of the instrument, we conclude that the performance of the interferometer is dominated by other sources of fundamental and technical noise in the detection band. We also give, under simplistic assumptions, an order-of-magnitude estimate for the maximum charge accumulation that could be tolerated near the test masses, revealing that a few  $\mu$ C of charge accumulation are enough to make the Johnson noise similar to the fundamental sources of noise for the interferometer.

We hope this article can serve as the first stepping stone in the way to a deeper understanding of the electrostatic environment surrounding the test masses in Advanced LIGO. The joint

<sup>&</sup>lt;sup>19</sup> This assumes the capacitor gap is the same as the space between the ESD and the test mass, 5 mm for the ETMs as per [34].

effort between modeling and measurement will be needed to tackle issues such as the effect of charge accumulation in the interferometers and beyond.

Furthermore, we believe the methods developed in this manuscript are also applicable to estimating the Johnson noise coupling from electrostatic actuators in third-generation observatories, like LIGO Voyager [39] or the Einstein Telescope [40]. The two main caveats stem from the fact that these projects plan to utilize cryogenically cooled silicon masses. First, the lower temperature implies that the circuitry of the electrostatic drive will not necessarily be in thermal equilibrium with the masses, hence violating one of the main assumptions of the fluctuation—dissipation theorem [27]. However, reasonable estimates can be made in non-equilibrium steady-state systems regardless of this fact [41], which we can immediately translate into this work. The second is that silicon is a semiconductor, and as such, it might violate the quasi-static assumptions made for this manuscript<sup>20</sup>. A more detailed analysis and simulation for the case of a semiconductor mass are part of the future research directions for the authors.

#### **Acknowledgments**

The authors gratefully acknowledge the support of the United States National Science Foundation (NSF) for the construction and operation of the LIGO Laboratory and Advanced LIGO as well as the Science and Technology Facilities Council (STFC) of the United Kingdom, and the Max-Planck-Society (MPS) for support of the construction of Advanced LIGO. Additional support for Advanced LIGO was provided by the Australian Research Council. This project was supported by NSF Grant PHY 17-08006. The authors acknowledge the LIGO Scientific Collaboration Fellows program for additional support. LIGO was constructed by the California Institute of Technology and Massachusetts Institute of Technology with funding from the National Science Foundation, and operates under cooperative agreement PHY-1764464. Advanced LIGO was built under award PHY-0823459. This article carries LIGO Document Number LIGO-P2000166.

#### Appendix A. Worked examples

In this appendix we demonstrate the use of the electromechanical equations to estimate the fluctuating force associated with the Johnson noise in simple electrostatic arrays. These examples serve to illustrate some of the general properties to be expected of general electromechanical systems in the electrostatic regime.

In all the examples, the key part of the estimation is finding the electromechanical coefficients  $\frac{\partial F_x}{\partial \phi}$  for the configuration. This can be done either directly by analyzing the forces of the system or indirectly through the electromechanical reciprocity (5). In each case, we take this result and plug it into our general estimate for the spectral density of the Johnson noise driven forces (10) to provide insight on the factors contributing to the Johnson noise coupling to mechanical motion.

In the first example we explore a simple system consisting of a point charge representing the movable object  $\mathcal{O}$  subject to the electrostatic force of a conductive plate. This example illustrates the most basic features of our framework.

 $<sup>^{20}</sup>$  It will ultimately depend on the relaxation time  $\tau = \rho \epsilon$  for the silicon mass. The strong dependence of silicon's resistivity on temperature and impurity concentration, in addition to the presence of field effects on surface conductivity [42] make this analysis a delicate one, outside the scope of this article.

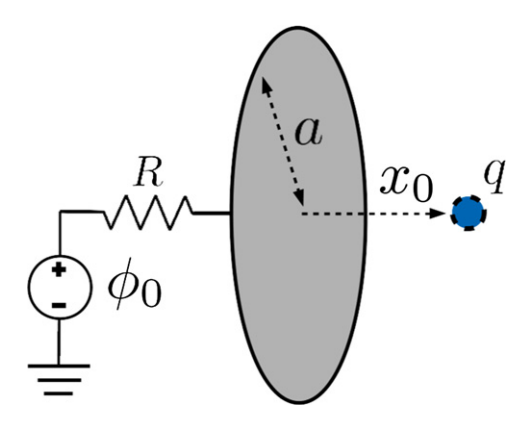


**Figure 6.** Conducting disk and point charge configuration. The point charge q is at a distance x from the center of the disk, which is connected to an ideal voltage source through a resistance R. The charge q is assumed to be held at an equilibrium position  $x_0$  when the source's potential is  $\phi_0$ .

In the second example we work with two conductive plates, one of them treated as the movable object  $\mathcal{O}$ , in order to show how capacitive forces are handled within the framework. In contrast with the point charge example the fluctuating force amplitude is found to be proportional to the potential difference  $\phi$ .

Finally, in the third example we explore the effect that a point charge q has on the parallel plate system of the second example, both when q is treated as a charge fixed in space near the object, and then when the charge is moved with, or attached to the object  $\mathcal{O}$ . In the latter case we can distinguish between three types of forces that act on the object  $\mathcal{O}$  which are all treated simultaneously by our framework.

In addition to illustrating the main features of our analysis, these toy models can serve as a proxy for the more complex environment around the LIGO test masses. We can leverage the developed knowledge to get a sense for what the interaction between the bias plate of the electrostatic drives and the Advanced LIGO test masses is in terms of simpler concepts like charges or capacitances. This enables us to give an order of magnitude estimate for the impact of free charge accumulation on the sensitivity of the interferometers, an estimation that is performed at the end of the examples by modeling the LIGO environment by the simplified configurations. For the purpose of these estimates, we will use the dimensions of the test and reaction masses, as specified in [34]. The test and reaction masses have a radius of 17 cm and are separated by a 5 mm vacuum gap.<sup>21</sup>. The test mass is 20 cm thick.

#### A.1. Conducting disk and point charge in axis of symmetry

Consider the scenario depicted in figure 6. A conductive plate of radius a is connected through a resistance R to an ideal voltage source with the potential fixed at  $\phi_0$ . We assume the charge q rests at an equilibrium distance  $x_0$  along the axis of symmetry of the disk when the potential is  $\phi_0$ .

<sup>&</sup>lt;sup>21</sup> The gap is 5 mm in the case of the end test masses (ETMs). The input test masses (ITMs) have a 20 mm gap instead.

From [16] we can obtain the self-capacitance of the disk and the electric force on the charge q as:

$$C_0 = 8\epsilon_0 a,\tag{17}$$

$$F_x(x,\phi) = \frac{2\phi}{\pi} \frac{qa}{x^2 + a^2},$$
 (18)

$$\left(\frac{\partial F_x}{\partial \phi}\right)_0 = \frac{2}{\pi} \frac{qa}{x_0^2 + a^2}.\tag{19}$$

From equation (10), the amplitude spectral density of the fluctuating force on the charge q is:

$$|F_{\eta}(f)| = \left(\frac{2}{\pi} \frac{qa}{x_0^2 + a^2}\right) \frac{\sqrt{4k_b TR}}{\sqrt{1 + (2\pi fRC_0)^2}}.$$
 (20)

There are three main aspects we would like to highlight from this expression. First, we can recognize the usual  $4k_BTR$  from the voltage fluctuations on the resistor. More generally, this numerator is directly proportional to the dissipative part of the circuits connected to the conductors.

Second, for low frequencies ( $f \ll 1/RC_0$ ) the fluctuating force's spectrum is independent of f, resembling white noise. When the charging time of the conductive plate (represented by  $\tau = RC_0$ ) is very long compared to the period of the fluctuating voltage (represented by 1/f) the conducting array acts as a low-pass filter and hence the force fluctuations on the charge q fall off as 1/f.<sup>22</sup>

Finally, we notice that the Johnson noise-induced force fluctuations go to zero both in the limit  $R \to 0$  and  $R \to \infty$ . The first case represents an ideal circuit with no dissipation, and hence no Johnson noise, whereas the second represents an ideal conductor disconnected from any circuits. There will be, for each frequency f, a value of R that *maximizes* the strength of the noise on that band. This fact could be used during the design phase to avoid impacting the important parts of the spectrum.

If we now assume that the conductive plate is the Advanced LIGO ESD and the point charge represents the test mass, we can obtain the displacement ASD from figure 5 with an equivalent charge of 130 nC. According to this approximation, an equivalent charge of 1.3  $\mu$ C on a single test mass would be enough for the Johnson noise to hit the baseline of the design sensitivity for Advanced LIGO.

However, considering the fact that there are two biased test masses, and their noises add up in quadrature to make up for most of the Johnson noise coupling shown in figure 5, a more refined estimate is that the equivalent charge for each test mass under this toy model is about 90 nC.

For Advanced LIGO, above the detection band, the frequency at which we expect to see the forces to fall as 1/f is driven by the 1 nF capacitor at the end of the bias circuit (see figure 4). This gives, for  $R=10~\mathrm{k}\Omega$ , a value of  $f=100~\mathrm{kHz}$ 

<sup>&</sup>lt;sup>22</sup> In general, the force fluctuations will be low passed due to the finite charge time of the circuits. The final frequency dependence will vary according to the linear circuits attached to the conductors in a more general array.

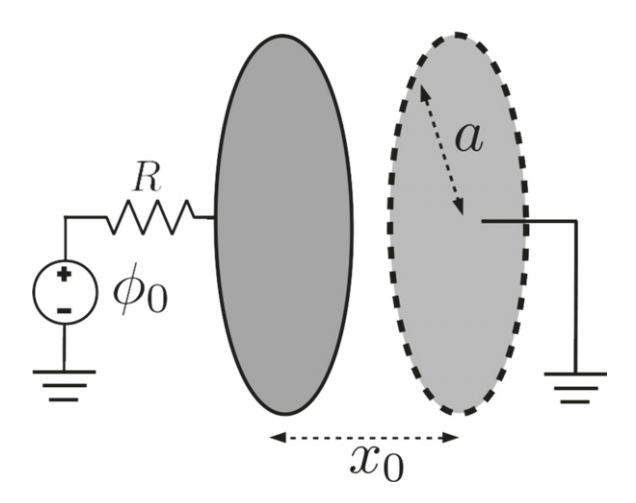


**Figure 7.** Parallel plate capacitor configuration. Both disks are of radius a. The left disk is connected to a reservoir potential through a resistance R while the right disk, treated as the object  $\mathcal{O}$ , is directly connected to the ground, maintaining the difference between them constant at  $\phi_0$ .

#### A.2. Purely capacitive forces: parallel plate capacitor

In a system with only linear capacitive couplings (no free charges), the electrostatic force on any object (conductors or dielectrics) is given by<sup>23</sup>:

$$F_x = \frac{1}{2} \left( \frac{\partial C}{\partial x} \right) \phi^2 \quad \Rightarrow \quad \left( \frac{\partial F_x}{\partial \phi} \right)_0 = \left( \frac{\partial C}{\partial x} \right)_0 \phi_0,$$
 (21)

where  $\frac{\partial C}{\partial x}$  represents the change on the total capacitance of the system when the involved object is moved along x. In the case of a parallel plate capacitor, like the one shown in figure 7,  $C(x) \propto \frac{1}{x}$  represents the mutual capacitance of the array while the potential  $\phi$  is the potential difference between the plates. The proportionality of C(x) implies that  $\left(\frac{\partial C}{\partial x}\right)_0 = -\frac{C_0}{x_0}$ . Consequently, after the application of equation (10), the amplitude spectral density of the

Consequently, after the application of equation (10), the amplitude spectral density of the fluctuating force on each plate is:

$$|F_{\eta}(f)| = \frac{C_0 \phi_0}{x_0} \sqrt{\frac{4k_b TR}{1 + (2\pi fRC_0)^2}}.$$
 (22)

An interesting property of capacitive systems is that the Johnson noise amplitude is proportional to the equilibrium potential  $\phi_0$ . This is due to the fact that the Johnson noise fluctuations exert forces on the induced charges, which are proportional to  $\phi_0$ .

The result shown in equation (22) is identical to an early estimate for the Advanced LIGO Johnson noise [13] in where the authors used an array similar to the one shown in figure 7, associating one plate with the electrostatic drive and the other with the Advanced LIGO test mass.

<sup>&</sup>lt;sup>23</sup> This is valid for any electrical system that can be described by a single potential  $\phi$ . The treatment for multiple potentials requires the capacitance matrix.

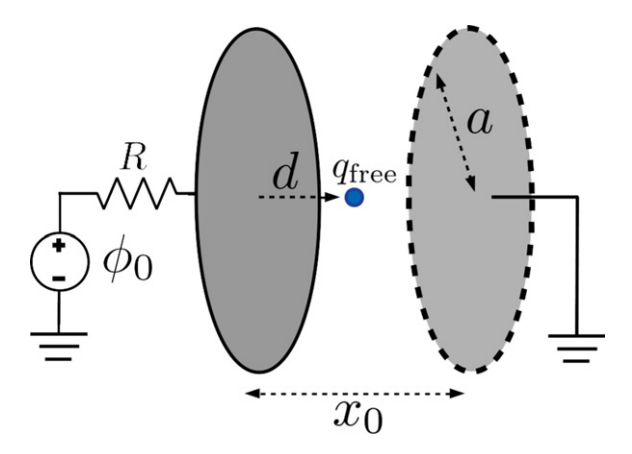


**Figure 8.** Parallel plate capacitor with point charge configuration. The left disk of radius a is connected to an ideal potential source through a resistance R, while the right plate is connected to the ground. At equilibrium, the potential is set to  $\phi_0$  and the distance between the plates is  $x_0$ . The point charge  $q_{\text{free}}$  is completely fixed at a distance d from one of the plates. In this configuration, we assume the right hand plate (shown with dashed lines) represents the object  $\mathcal{O}$  to which we apply the electromechanical equations.

If we use this approximation, in order to reproduce the contribution of the Johnson noise  $(\approx 4 \times 10^{-19} \text{ at } 10 \text{ Hz})$  to the position ASD (shown in figure 5) with the parallel plate model we need to set the effective capacitance of the two biased masses to be  $C_0 \approx 5 \text{ pF.}^{24}$ . With the usual values for the bias potential  $\phi_0 \approx 400 \text{ V}$  (from table 1) this corresponds to an induced charge of  $Q_0 = C_0 \phi_0 \approx 2 \text{ nC}$ .

To achieve the same level of noise the total induced charge is an order of magnitude less than the obtained in the previous point charge model. The difference can be accounted for by the different dependencies of the electric forces with the separation between the test and reaction masses. Since the capacitance in this example scales as  $\frac{1}{x}$ , a small separation such as  $x_0 = 5$  mm boosts the force considerably.

In this sense, while the parallel plate model captures the essence of the test mass polarization by the electrostatic drive, the assumption that  $C(x) \propto \frac{1}{x}$  is clearly invalid. Nevertheless, the parallel plate toy model is good enough to illustrate the effect of free charges in the Johnson noise amplitude, as we show in the next section.

#### A.3. Parallel plate capacitor in the presence of a point charge

Similar to the previous example, we have a parallel plate capacitor, but this time there is a point charge q present in the array. Figure 8 shows the basic arrangement in where the charge  $q_{\text{free}}$  is located at a distance d from one of the conducting plates and does not move. Our 'object'  $\mathcal{O}$  is once again the other plate, represented with dashed lines in the figure.

Under these assumptions, the total charge on the plate connected to the resistance is:

$$q = C\phi + q_{\text{imag}}. (23)$$

<sup>&</sup>lt;sup>24</sup> This assumes that the gap size  $x_0 = 5$  mm as per [34].

The charge  $q_{\rm imag}$  is the charge induced by the presence of the point charge  $q_{\rm free}$  when both plates are grounded<sup>25</sup>. If we assume the dimension of the plates is much larger than their separation, and that the charge  $q_{\rm free}$  is close to the axis of symmetry of the two plates, we can treat the array as two infinite plates. Then, we can find the geometric potential at the point charge's location (see appendix C) to be  $f=1-\frac{d}{x}$ . Using equation (14) we find the charge on the left plate  $q_{\rm imag}$ :

$$q_{\text{imag}} = -q_{\text{free}} \left( 1 - \frac{d}{x} \right). \tag{24}$$

We can then use the electromechanical relation (5) and the expression for the charge  $q_{\rm imag}$  to find the force derivative:

$$\left(\frac{\partial F_x}{\partial \phi}\right)_0 = \left(\frac{\partial q}{\partial x}\right)_0 = \left(\frac{\partial C}{\partial x}\right)_0 \phi_0 - \frac{q_{\text{free}}d}{x_0^2}.$$
 (25)

The term  $\frac{\partial C}{\partial x}$  was already calculated on the previous example and still holds. Note that the geometric potential approach saved us the trouble of having to use the images method to explicitly calculate the induced charge distribution on any of the plates.

Plugging this result in equation (10) to get the spectral density of the force, we obtain:

$$|F_{\eta}(f)| = \left| \frac{C_0 \phi_0}{x_0} + \frac{q_{\text{free}} d}{x_0^2} \right| \sqrt{\frac{4k_b TR}{1 + (2\pi fRC_0)^2}} = \left| \frac{Q_{\mathcal{O},0}}{x_0} \right| \sqrt{\frac{4k_b TR}{1 + (2\pi fRC_0)^2}}.$$
(26)

The last equality comes from recognizing that the total charge induced on the plate that represents the 'object' of interest  $\mathcal{O}$  (right plate in figure 8) is given by:

$$Q_{\mathcal{O}} = -C\phi - q_{\text{free}}\frac{d}{x}.$$
 (27)

This results implies that the magnitude of the force associated with Johnson noise is proportional to the total induced charge on the plate representing the object  $\mathcal{O}$ .

From this calculation we would like to highlight some interesting points about the effect of free charges on the Johnson noise coupling.

First, we can see that the effect of the free charges on the Johnson noise coupling is independent on the equilibrium potential  $\phi_0$ . The reason for this is that the magnitude and distribution of the charges induced in  $\mathcal{O}$  by any free charge density  $\rho_{\text{free}}$ , at the equilibrium position of the array, is independent of the potential.

Second, we notice that the presence of the free charge had a net effect in the magnitude of the Johnson noise even though it did not form part of the moving object O. We can conclude that in a more general system free charges will have a direct effect on the magnitude of the force noise even if they are not attached to the moving objects.

Third, the presence of free charges could potentially counteract the contribution from the potential  $\phi_0$ , depending on the magnitude and sign of  $q_{\rm free}$ .<sup>26</sup>

 $<sup>^{25}</sup>$  It can be helpful to think about these as the image charges induced by  $q_{\mathrm{free}}$  on the conductive plate.

 $<sup>^{26}</sup>$  More generally, it will depend on the specifics of the charge distribution  $\rho_{\rm free}$  and the geometry of the system.

Fourth, the magnitude of the effect caused by  $q_{\text{free}}$  goes to zero if  $d \to 0$ . In this situation, the charge is completely screened by the other conductor and it is equivalent to the charge not being present.

Finally, the noise effect grows as the charge  $q_{\text{free}}$  is closer to  $\mathcal{O}$ , since doing this increases the amount of charge induced on the plate. However, the situation changes if the charge is *attached* (belongs) to the plate, as we explore in the following subsection.

A.3.1. Charge attached to the conductive plate. Let us consider the case where the point charge  $q_{\text{free}}$  is 'attached' to the conducting test mass at its position, such that  $\Delta d = \Delta x$ . This implies that from the mechanical point of view, the object  $\mathcal{O}$  is comprised by not only the right hand plate from figure 8 but also the free charge  $q_{\text{free}}$  as a singular rigid body.

We can immediately include the effect of forces on this charge by including the derivative of d with respect to x in equation (25):

$$\left(\frac{\partial F_x}{\partial \phi}\right)_0 = \left(\frac{\partial q}{\partial x}\right)_0 = \left(\frac{\partial C}{\partial x}\right)_0 \phi_0 - \frac{q_{\text{free}}d}{x_0^2} + \frac{q_{\text{free}}}{x_0} \left(\frac{\partial d}{\partial x}\right)_0 \\
= -\frac{C_0 \phi_0}{x_0} - \frac{q_{\text{free}}d}{x_0^2} + \frac{q_{\text{free}}}{x_0}.$$
(28)

We recognize three different components on the right-hand side of equation (28) which will contribute to the total effect of the Johnson noise. All three components are forces that the left plate applies on the object  $\mathcal{O}$ , but they have different interpretations:

- The first term relates to the capacitive force on the charges induced by the potential difference  $\phi_0$ .
- ullet The second is the force on the image charges induced by the free charge  $q_{\mathrm{free}}.$
- The third one is the force on the free charge  $q_{\text{free}}$  itself, which now forms part of the object  $\mathcal{O}$  due to the constraint  $\Delta d = \Delta x$ .

This analysis highlights the power of the electromechanical reciprocity relation (5), since we have treated the three different forces simultaneously, without the need to find or integrate charge distributions.

If the point charge is attached to the surface of the right plate then  $d=x_0$  and the sum of the forces on the charge  $q_{\rm free}$  and its image in  $\mathcal O$  cancels. This is to be expected, since for  $d=x_0$  the test mass's image charge perfectly screens the charge  $q_{\rm free}$ .

In the case of Advanced LIGO, the test mass is not a conductor but a dielectric. This implies that there is never a complete screening of the charge  $q_{\rm free}$ . Nevertheless, we can use the knowledge we have gathered from the toy models to increase our understanding of the real arrangement.

#### A.4. Notes on dielectrics

While the general approach used for the previous examples still applies for an array of conductors and dielectrics, it must be noted that it is complicated to make a meaningful approximation without knowledge about the specific geometry in which the conductor and dielectrics are arranged, since dielectrics do not have a set potential.

These constraints prevent us from making an example that is both analytic and accurately illustrates the way that conductors and dielectrics interact in the actual array present

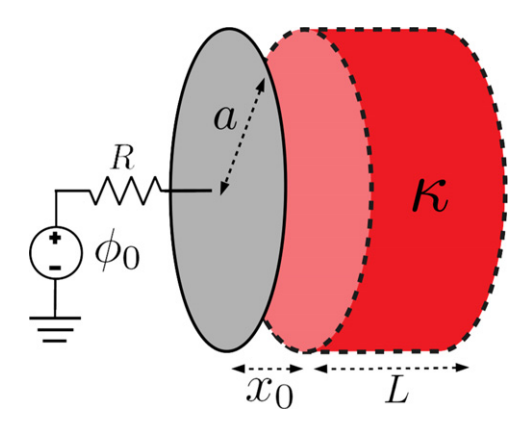


Figure 9. Conducting disk and dielectric configuration. One of the faces of a dielectric cylinder is placed at a distance x from a circular conductive plate. The conductor is connected to an ideal voltage source through a resistance R. The dielectric is assumed to be at an equilibrium position  $x_0$  when the source's potential is  $\phi_0$ . In this configuration, we assume the dielectric cylinder (shown with dashed lines) represents the object  $\mathcal{O}$  to which we apply the electromechanical equations.

in Advanced LIGO. Numerical simulations are required even for the simple model shown in below.

Therefore, for this section, we will limit ourselves to a qualitative analysis of the system shown in figure 9: a circular plate of radius a is connected through a resistance R to an ideal voltage source with the potential fixed at  $\phi_0$ . A dielectric cylinder with the same radius and dielectric constant  $\kappa$  is placed with one of its circular faces at a distance  $x_0$  from the conductive plate.

The forces on the dielectric are purely capacitive in nature, so we expect equation (21) to apply, hence  $\left(\frac{\partial F_x}{\partial \phi}\right)_0 = \left(\frac{\partial C}{\partial x}\right)_0 \phi_0$ . Similarly, we also know that the capacitance of the array is increased by the presence of the

dielectric slab. It should lie somewhere in between the vacuum capacitance and the capacitance if space was filled with a dielectric of constant  $\kappa$ . That is:  $8\epsilon_0 a < C_0 < 8\epsilon_0 \kappa a$ .

We also expect the capacitance to not diverge as the distance  $x_0$  goes to zero. Considering

the other relevant length scales of the problem we can estimate that  $\left|\frac{\partial C}{\partial x}\right|_0 \approx \frac{C_0}{L}$  if  $L \gg x_0.^{27}$  If we plug the numbers for the advanced LIGO masses and with  $\kappa = 3.8$  for fused silica, we obtain an approximate value of  $\left|\frac{\partial F_x}{\partial \phi}\right|_0 \approx 1 \times 10^{-7}$  N V<sup>-1</sup>, which is on the same order of magnitude of the values from the biased masses on table 2.

As mentioned above, we cannot expect more than an order-of-magnitude estimate for the actuation strength, since the specific values will depend on the geometry of the system. Nevertheless it is important to note that a simplification like this can yield a better back of the envelope estimate for the actuation strength than the parallel-plate capacitor model.

<sup>&</sup>lt;sup>27</sup> Numerous tractable toy models exhibit this same behavior, such as the parallel plate capacitor partially filled with a dielectric medium.

#### Appendix B. Electromechanical reciprocity relations

In this appendix we derive the electromechanical reciprocity relation shown in equation (5) from first principles, that is:

$$\frac{\partial \vec{\mathbf{q}}}{\partial \vec{\mathbf{r}}} = \left[ \frac{\partial \vec{\mathbf{F}}}{\partial \vec{\Phi}} \right]^{\mathrm{T}}.$$
 (29)

This important equation relates  $\frac{\partial q_i}{\partial r_k}$ , the partial derivative of the charge stored in conductor  $C_i$  by moving an object in the direction  $r_k$  and keeping the potentials  $\vec{\phi}$  constant, with  $\frac{\partial F_k}{\partial \phi_i}$ , the derivative on the force in direction  $r_k$  acting on the same object by changing the potential  $\phi_i$  of the same conductor  $C_i$  by keeping the position of the object  $\vec{r}$  constant.

We start by computing the electric energy of the system  $U(\vec{q}, \vec{r})$  and then derive the free energy  $\tilde{U}(\vec{\phi}, \vec{r})$ . We then show that the electromechanical reciprocity relation follows from considering second derivatives of  $\tilde{U}$ .

#### B.1. Internal energy of a system of conductors, charges and dielectrics

The total electric energy contained in a system of conductors, charges and dielectrics is:

$$U = \frac{1}{2} \int \vec{E} \cdot \vec{D} \, d^3 \vec{r} = -\frac{1}{2} \int (\nabla \phi) \cdot \vec{D} \, d^3 \vec{r}$$
$$= -\frac{1}{2} \left( \int \nabla \cdot (\phi \vec{D}) \, d^3 \vec{r} - \int \phi \nabla \cdot \vec{D} \, d^3 \vec{r} \right), \tag{30}$$

where  $\vec{E}$  and  $\vec{D}$  are the electric and displacement field respectively, and the volume integrals are over all space<sup>28</sup>.

Using Gauss' law the first integral becomes zero since  $\phi$  is defined to be zero at infinity. For the second integral, since  $\nabla \cdot \vec{D} = \rho_{\text{free}}$  we will have two types of terms: those relating the free charge on the surface of the conductors and those relating to the free charges in the rest of space. The former simplifies since the conductors are at constant potential and we obtain:

$$U = \frac{1}{2} \left( \sum_{i} \phi_{i} q_{i} + \int \phi \rho_{\text{free}} \, d^{3} \vec{r} \right). \tag{31}$$

Here, the sum is over the conductors and the integral is over the free charge density not associated with any conductor.

#### B.2. Conjugate variables for U and the associated free energy $\tilde{U}$

As it is done in Landau and Lifshitz's *Electrodynamics* [16] we can express the change in the energy U due to a change of the conductors' charge by  $dq_i$ , assuming that all dielectrics are

<sup>&</sup>lt;sup>28</sup> The arguments of this section still hold if the system is enclosed inside another conductor  $C_{N+1}$  (for example, the vacuum chamber in Advanced LIGO). The caveat is that the potential of this conductor has to be set as the reference potential  $\phi_{N+1} = 0$ .

linear<sup>29</sup>:

$$dU = \sum_{i} \phi_{i} dq_{i}. \tag{32}$$

Since the potential U is written as a function of the independent charges in the conductors we conclude that  $\phi_i = \left(\frac{\partial U}{\partial q_i}\right)$ .

These ideas are explored further in Landau and Lifshitz's *Electrodynamics* pp 30 [16] in which the authors justify the introduction of a modified potential energy  $\tilde{U}$  that is a function of the potentials on the conductors:

$$\tilde{U} = U - \sum_{i} \phi_{i} q_{i} = \frac{1}{2} \left( \int \phi \rho_{\text{free}} d^{3} \vec{r} - \sum_{i} \phi_{i} q_{i} \right), \tag{33}$$

which represents the free energy available to the system when we consider it as a function of the independent potentials  $\vec{\phi}$ .<sup>30</sup>

Using this formalism, the forces due to displacing any object inside the arrangement of conductors can be calculated through either U or  $\tilde{U}$  and the result should be the same, yielding:

$$F_k = -\left(\frac{\partial U}{\partial r_k}\right)_{q_i} = -\left(\frac{\partial \tilde{U}}{\partial r_k}\right)_{\phi_i}.$$
 (34)

Note also, that since  $\tilde{U}$  is a Legendre transform of U then  $q_i = -\left(\frac{\partial \tilde{U}}{\partial \phi_i}\right)$ , which can be verified by plugging equation (44) into the definition for  $\tilde{U}^{31}$ . A bit of attention must be taken, the partial derivatives assume all of the generalized coordinates are kept constant. We will drop the subscripts for now, with the knowledge that U is a function of the positions and charges, while  $\tilde{U}$  is a function of the positions and potentials.

#### B.3. Electromechanical reciprocity

Having defined the free energy  $\tilde{U}$  we can finally prove equation (5). Since by equation (34) the force on an object  $F_k$  is a first derivative of  $\tilde{U}$  then  $\left(\frac{\partial F_k}{\partial \phi_i}\right)$  involves second derivatives of  $\tilde{U}$ . It is then straightforward to see that:

$$\left(\frac{\partial F_x}{\partial \phi_i}\right) = -\frac{\partial^2 \tilde{U}}{\partial \phi_i \partial r_k} = -\frac{\partial^2 \tilde{U}}{\partial r_k \partial \phi_i} = \left(\frac{\partial q_i}{\partial r_k}\right).$$
(35)

As we have mentioned earlier, this relation implies that the rate of change of the net force on an object when changing the value of the surface equipotential of a given conductor is equal to the rate of change of the equilibrium charge of the conductor when displacing the object on the direction of the force.

<sup>&</sup>lt;sup>29</sup> The factor  $\frac{1}{2}$  in equation (31) is not present in equation (32) as one might naively guess if the differential operator is applied considering the potentials  $\phi_i$  to be independent from the change in the charges. We must remember that the derivative  $\frac{\partial \phi_i}{\partial q_j} = (\mathbf{C}^{-1})_{ij} \neq 0$ .

 $<sup>^{30}</sup>$   $\tilde{U}$  arises since it is impossible to keep the potentials of the conductors constant during a mechanical transition without exchanging charge with the environment. This is similar to the definition for enthalpy from thermodynamics. The enthalpy arises since it is impossible to increase the temperature of a gas at constant pressure without it doing work on its surroundings.

<sup>&</sup>lt;sup>31</sup> Alternatively, this relationship can be taken as the definition of the total charge in the conductors, which yields the same result as (44) for linear systems.

Another useful, and almost equivalent relation is:

$$\left(\frac{\partial F_k}{\partial q_i}\right) = -\frac{\partial^2 U}{\partial q_i \partial r_k} = -\frac{\partial^2 U}{\partial r_k \partial q_i} = -\left(\frac{\partial \phi_i}{\partial r_k}\right).$$
(36)

We can write similar relations for each coordinate motion. Furthermore, these relations also hold for angular degrees of freedom. Using the definition for the torque:  $\tau_k = -\left(\frac{\partial U}{\partial \theta_k}\right) = -\left(\frac{\partial \tilde{U}}{\partial \theta_k}\right)$ , we find that:

$$\left(\frac{\partial \tau_k}{\partial \phi_i}\right) = \left(\frac{\partial q_i}{\partial \theta_k}\right) \quad \text{and} \quad \left(\frac{\partial \tau_k}{\partial q_i}\right) = -\left(\frac{\partial \phi_i}{\partial \theta_k}\right).$$
(37)

#### Appendix C. Modelling the electromechanic coefficients

In this appendix we prove equation (14) used in section 4 to calculate the charge induced in each conductor due to the presence of free charge distributions. The backbone of the proof uses an extension of the Green's reciprocity relation (see [43]) that relates the charge distributions  $\rho_1$  and  $\rho_2$  and the electric potentials  $\phi_1$  and  $\phi_2$  of two different system configurations that share the same geometry in terms of conducting surfaces.

The usual statement of the Green's reciprocity theorem is made in the absence of dielectrics. We show that if the dielectrics involved are linear, then the proposition of the theorem it is still true for the free charge density  $\rho_{\rm free}$ .

We then use the equation derived to illustrate the steps necessary to estimate the electromechanical coefficients (5) from a finite element simulation by leveraging the geometric potentials of an electrostatic array with no free charges.

#### C.1. Green's reciprocity in the presence of linear dielectrics

Consider a system of N conductors, with linear dielectrics and free charges, bounded by an external conductor  $C_{N+1}$ . The potential of the external conductor is set to be zero (or as the reference potential) for the remainder of this proof<sup>32</sup>.

For a given single spatial configuration of the system of conductors and dielectrics, Maxwell's equations for electrostatics can be used to describe the electric interactions. The equations can be summarized as:

$$\nabla \cdot (\hat{\epsilon} \nabla \phi) = -\rho \quad ; \quad \phi = \phi_i \text{ (constant)} \quad \text{in } C_i.$$
 (38)

The first equation includes the spatially varying electric permittivity  $\hat{\epsilon}$  in its most general form as a rank-two symmetric tensor [16], this accounts for the effect of dielectrics anywhere in space. It is satisfied in the volume enclosed by  $\mathcal{C}_{N+1}$ . The second one provides the boundary conditions for the electrostatic potential  $\phi$  inside the conductors.

The charge density  $\rho$  considered in equation (38) is that of all conductors plus any free charge density  $\rho_{\text{free}}$  present in the system, not including the bound charge due to polarization of the dielectrics, since the information regarding the possible existence of these polarization charge densities is encoded in  $\hat{\epsilon}$ .

<sup>&</sup>lt;sup>32</sup> This is the natural choice, since in the absence of free charge density, if all the conductors' potentials match the enclosure's the electric field inside has to be zero.

Let us consider two different free charge distributions  $\rho_1(\vec{r})$  and  $\rho_2(\vec{r})$  with their associated potentials  $\phi_1(\vec{r})$  and  $\phi_2(\vec{r})$  of this system. The potentials both satisfy the equation (38). We can find a relation between the two distributions by partial integration on the following equation:

$$\int_{\mathcal{V}} \phi_2 \rho_1 d^3 \vec{r} = -\int_{\mathcal{V}} \phi_2 \nabla \cdot (\hat{\epsilon} \nabla \phi_1) d^3 \vec{r} = \int_{\mathcal{V}} \left[ \nabla \phi_2 \cdot (\hat{\epsilon} \nabla \phi_1) - \nabla \cdot (\phi_2 \hat{\epsilon} \nabla \phi_1) \right] d^3 \vec{r}.$$
(39)

If we take the integration domain  $\mathcal{V}$  to be the inside of the exterior conductor  $\mathcal{C}_{N+1}$ , then the last term on the right-hand side of equation (39) is zero, due to Gauss' law and our convention where the potential of the outer conductor is set to zero. On the other hand, the other term satisfies  $\nabla \phi_2 \cdot (\hat{\epsilon} \nabla \phi_1) = \nabla \phi_1 \cdot (\hat{\epsilon} \nabla \phi_2)$  due to the symmetry of the permittivity tensor.

Continuing with a second integration by parts, and making use of the fact that the two distributions share the same geometry:

$$\int_{\mathcal{V}\nabla} \phi_1 \cdot (\hat{\epsilon} \nabla \phi_2) d^3 \vec{r} = \int_{\mathcal{V}} \left[ \nabla \cdot (\phi_1 \hat{\epsilon} \nabla \phi_2) - \phi_1 \nabla \cdot (\hat{\epsilon} \nabla \phi_2) \right] d^3 \vec{r} = \int_{\mathcal{V}} \phi_1 \rho_2 d^3 \vec{r}. \tag{40}$$

Where we have again used the reference potential convention to eliminate the boundary term and equation (38) to write the integral in terms of the charge density. The final result is then:

$$\int_{\mathcal{V}} \phi_2 \rho_1 \mathbf{d}^3 \vec{r} = \int_{\mathcal{V}} \phi_1 \rho_2 \mathbf{d}^3 \vec{r}. \tag{41}$$

Which is the usual known form of the Green's reciprocity theorem [23]. Note, however that in the usual statement of the theorem, the densities  $\rho$  correspond to the *total* charge density on an arbitrary configuration of charges. The expression (41) involves two arbitrary configurations of *free* charge density, provided that the conductors and dielectrics (which affect  $\hat{\epsilon}$ ) remain in the same positions.

#### C.2. Charge induced by a free charge distribution $\rho_{\text{free}}$

We will apply the green reciprocity relation to estimate the effect that a free charge distribution  $\rho_{\text{free}}$  has on the total charge of the conductors of the system.

Given an array like the one shown in figure 10, let us consider two situations:

- (a) The first one with all the conductors grounded and the free charge  $\rho_{\text{free}}$  present. Let  $q_i$  denote the total charge of conductor i induced by the free charge density in this grounded configuration.
- (b) The second one with all but one conductor grounded. Let us assume that the ungrounded conductor is conductor i and its potential is denoted by  $V_0$ . The potential in the rest of the array is denoted by  $\phi_i(\vec{r})$ . No extra free charge density is present in this configuration.

Equation (41) applied to these two situations yields:

$$q_i V_0 + \int_{\mathcal{V}} \rho_{\text{free}}(\vec{r}) \phi_i(\vec{r}) d^3 \vec{r} = 0.$$

$$\tag{42}$$

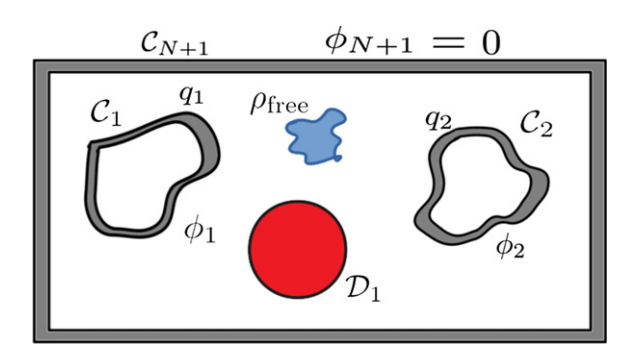


**Figure 10.** System consisting of conductors  $C_i$ , dielectrics  $D_j$  and free charge density  $\rho_{\text{free}}$ .

Note that the right-hand side of equation (42) is identically zero, since situation 1 has the potentials on the conductor surfaces equal to zero and situation 2 has no free charge densities not attached to conductor surfaces.

The induced charge  $q_i$  by the free charge  $\rho_{\text{free}}$  in conductor  $C_i$  is then given by:

$$q_{i} = -\frac{1}{V_{0}} \int_{\mathcal{V}} \rho_{\text{free}}(\vec{r}) \phi_{2}(\vec{r}) d^{3} \vec{r} = -\int_{\mathcal{V}} \rho_{\text{free}}(\vec{r}) f_{i}(\vec{r}) d^{3} \vec{r}.$$
(43)

Where we have defined the geometric potentials  $f_i(\vec{r}) = \frac{\phi_i}{V_0}$  associated with conductor i, as defined in [44]. These are defined as the normalized potentials for the configuration (b) mentioned before, with only conductor i ungrounded.

By applying the superposition principle we can compute the total induced charges on the conductors  $\vec{q}$  as the sum of the charges generated by the free charge distributions in the system  $\rho_{\text{free}}$  plus the charges induced by the set of potentials on the conductors through the capacitance matrix:

$$\vec{q} = \mathbf{C}\vec{\phi} - \int_{\mathcal{V}} \rho_{\text{free}}(\vec{r})\vec{f}(\vec{r})d^{3}\vec{r}.$$
 (44)

#### C.3. Obtaining the electromechanical coefficients

In order to obtain the effect of free charges on the electromechanical coefficients  $(\frac{\partial \mathbf{q}}{\partial \mathbf{r}})$  we need to take the derivative of equation (44), the accumulated charge on the conductors, with respect to rigid body motions of an object  $\mathcal{O}$ .

First, we need to define a coordinate system representing the frame of reference of  $\mathcal{O}$ . Translations and rotations of  $\mathcal{O}$  will all be referenced to translations and rotations of this coordinate system instead.

Let us consider a rigid body translation along a direction  $r_k$  first:

$$\frac{\partial q_i}{\partial r_k} = \sum_j \frac{\partial C_{ij}}{\partial r_k} \phi_j - \int_{\mathcal{V}} \frac{\partial \rho_{\text{free}}}{\partial r_k} f_i(\vec{r}') d^3 \vec{r'} - \int_{\mathcal{V}} \rho_{\text{free}}(\vec{r'}) \frac{\partial f_i}{\partial r_k} d^3 \vec{r'}. \tag{45}$$

The first and last terms of this equation contain derivatives that are completely independent of the free charge distribution  $\rho_{\text{free}}$ . In fact, if  $\mathcal{O}$  is only composed of free charges, they are identically zero. On the other hand, the middle term only contributes if the moving object contains any of the free charge density.

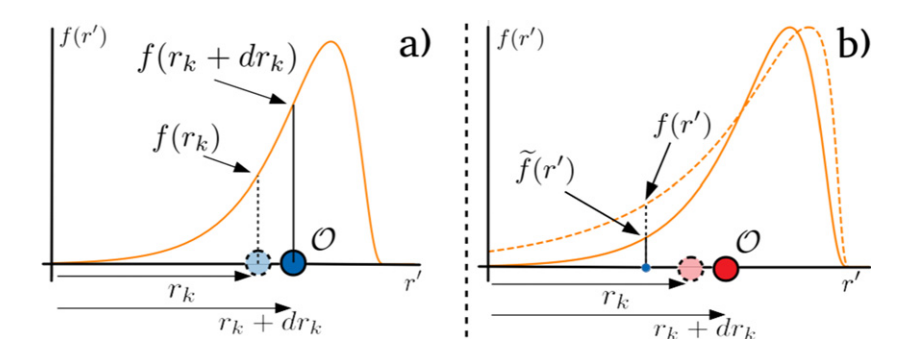


**Figure 11.** Simplified examples of the behavior of the integrands in the last two terms in equation (46) in one dimension. (a) The object  $\mathcal{O}$  consisting of free charges (in blue) is moved from  $r_k$  to  $r_k + dr_k$ . The function f(r') does not change overall by this movement but now the object's free charge is in another position, offset by an amount  $dr_k$ , where f(r') has a different value. The net effect is captured by the gradient of f in the  $\hat{e}_k$  direction. (b) The object  $\mathcal{O}$  consists of a dielectric (red) and is moved from  $r_k$  to  $r_k + dr_k$ . The function f(r') now changes overall since it depends on the position of all the conductors and dielectrics. On the third integral of equation (45) the free charge at position r', which did not move, gets multiplied by a different value under the integration  $\widetilde{f}(r')$ . This modified function is such that  $\frac{\widetilde{f}(r') - f(r')}{dr_k} \approx \frac{\partial f(r')}{\partial r_k}$ . The final result (46) for a general object is the superposition of these two effects.

Let  $\rho_o$  be the subset of the charge  $\rho_{\rm free}$  that is part of  $\mathcal{O}$ . The middle integral in equation (45) can be simplified by performing the derivative of the charge density in a step-by step basis (see figure 11). The resulting quantity is the gradient of  $f_i$  along the direction set by  $r_k$  (here denoted by  $\hat{e}_k$ ). We have therefore:

$$\frac{\partial q_i}{\partial r_k} = \sum_i \frac{\partial C_{ij}}{\partial r_k} \phi_j - \int_{\mathcal{V}} (\nabla f_i \cdot \hat{e}_k) \rho_o(\vec{r'}) d^3 \vec{r'} - \int_{\mathcal{V}} \rho_{\text{free}}(\vec{r'}) \frac{\partial f_i(r')}{\partial r_k} d^3 \vec{r'}. \tag{46}$$

By virtue of the electromechanical reciprocity relations (5),  $\frac{\partial q_i}{\partial r_k} = \frac{\partial F_k}{\partial \phi_i}$ . Hence, we can interpret the meaning of the terms on equation (46) as the different potential-dependent forces acting on  $\mathcal{O}$ :

- The first one corresponds to the forces between the charges on the surfaces of every conductor and the charges induced on the object  $\mathcal{O}$  by the potentials  $\vec{\phi}$ . It is zero if  $\mathcal{O}$  is comprised only of free charges (and thus cannot be charged or polarized).
- The second term is the force on the free charges that are part of  $\mathcal{O}$ . It is proportional to the geometric electric fields  $\nabla f_i$  at the position of the charges.
- The last term is the force between the charges induced by the potentials  $\vec{\phi}$  and the ones induced by the free charge density  $\rho_{\text{free}}$ .

It is important to note that the force between  $\rho_{\text{free}}$  and the charge it induces on  $\mathcal{O}$  is missing from the list, since it does not depend on the potentials  $\vec{\phi}$ .

In the case of a rotation, a similar analysis yields:

$$\frac{\partial q_i}{\partial \theta_k} = \sum_j \frac{\partial C_{ij}}{\partial \theta_k} \phi_j - \int_{\mathcal{V}} \left[ (\vec{r} - \vec{r}_o) \times \nabla f_i \right] \cdot \hat{e}_k \ \rho_o(\vec{r}) d^3 \vec{r} - \int_{\mathcal{V}} \rho_{\text{free}}(\vec{r}) \frac{\partial f_i}{\partial \theta_k} d^3 \vec{r}. \tag{47}$$

Here  $\vec{r}_o$  represents the position of the origin of the rotating coordinate system and  $\hat{e}_k$  represents the unitary vector along the axis of rotation. Using the electromechanical reciprocity:  $\frac{\partial q_i}{\partial \theta_k}$  $\frac{\partial \tau_k}{\partial \phi_i}$ , we conclude this is how we study the sensitivity of the angular degrees of freedom to electrostatic actuation.

#### C.4. Leveraging finite element modelling

From equations (46) and (47), we can see that in order to evaluate the effect of free charges in the electromechanic coefficients, it is sufficient to model the derivatives and gradients of  $f_i$  and  $C_{ij}$ . All of this quantities can be obtained from modelling an electrostatic array with no free charge density  $\rho_{\rm free}$ . Let us quickly outline the method for assembling the necessary pieces to obtain them:

- The geometric potentials  $f_i$  and their gradients  $\nabla f_i$  can be obtained for all space by modelling the electrostatic environment with all conductors grounded, with the exception of conductor i which is set to a potential of unity. The sets of conductors C, dielectrics D and objects  $\mathcal{O}$ , are located at their equilibrium positions.
- The capacitance matrix can be modelled in a similar way to the previous point. The procedure is standard, an example explanation for it can be found in [24].
- The derivatives  $\frac{\partial C_{ij}}{\partial r_k}$  and  $\frac{\partial f_i}{\partial r_k}$  can be approximated for a single object in  $\mathcal{O}$  by repeating the modelling from the previous two bullet points but with the object displaced a small amount  $\Delta r_k$  in the  $\hat{e}_k$  direction. Then we can approximate the derivatives by comparing the displaced values with the equilibrium ones:  $\frac{\partial C_{ij}}{\partial r_k} \approx \frac{\Delta C_{ij}}{\Delta r_k}$  and  $\frac{\partial f_i}{\partial r_k} \approx \frac{\Delta f_i}{\Delta r_k}$ .

  • In order to evaluate the effect of an arbitrary charitred values for  $\nabla f_i$  and  $\frac{\partial f_i}{\partial r_k}$  and integrate them
- with the charge distribution as in equations (46) and (47).
- The number of simulations needed per object in order to be able to store the necessary parameters is at most  $2N_{\text{dof}}$  ( $|\mathcal{C}| + 1$ ).<sup>33</sup> Then, we can compare the effect of arbitrary distributions by integrating over the stored parameters.
- In contrast, if we naively tried to estimate  $\frac{\partial F_k}{\partial \phi_i}$  for a single distribution we would need  $2|\mathcal{C}|$  simulations. Adding up all degrees of freedom it yields  $2N_{\text{dof}}|\mathcal{C}|$  simulations for one charge distribution  $\rho_{\rm free}$ . The advantage of the method outlined is that it allows us to store the relevant physical parameters to compare multiple charge distributions with ease.

#### C.5. Notes on potential dependent forces and charge effects in advanced LIGO

An interesting consequence of equation (46), through the electromechanical reciprocity is that we can find an explicit form for the electrostatic forces acting on an object  $\mathcal{O}$  in the direction of  $\hat{e}_k$  as:

$$F_{k} = \vec{\phi}^{\top} \frac{\partial \mathbf{C}}{\partial r_{k}} \vec{\phi} - \left( \int_{\mathcal{V}} \left( \nabla \vec{f} \cdot \hat{e}_{k} \right) \rho_{o}(\vec{r'}) d^{3} \vec{r'} + \int_{\mathcal{V}} \rho_{\text{free}}(\vec{r'}) \frac{\partial \vec{f}(r')}{\partial r_{k}} d^{3} \vec{r'} \right) \cdot \vec{\phi} + F_{0}, \quad (48)$$

where  $F_0$  is a electrostatic force independent of the potentials (for example free charge attracting a dielectric object).

 $<sup>^{33}</sup>N_{
m dof}$  is the number of mechanical degrees of freedom of the object.  $|\mathcal{C}|$  is the number of conductors. This assumes we need to model each geometric potential and the capacitance matrix separately, a worst case scenario, since the capacitance matrix and the geometric potentials are related by an integral equation [44].

Note that the vector  $\vec{\phi}$  is just a list of the potentials of the conductors in the array. Note that in this expression, the reference potential is set to be the potential of the surrounding conductor (as in figure 10).

In a system like the Advanced LIGO test masses and electrostatic drives, we are interested in the longitudinal actuation from two potentials: the bias electrode potential  $V_b$  and the signal electrodes' potential  $V_s$  if they are all driven in unison. The potential of other conductors is considered constant and not relevant for actuation.

Under these assumptions let us define  $\Phi$  as the list of all other conductor potentials that are not part of the ESDs<sup>34</sup>. Expanding equation (48) for longitudinal actuation and writing it with  $V_b$  and  $V_s$  as variables yields:

$$F_{x} = AV_{b}^{2} + BV_{b}V_{s} + CV_{s}^{2} + DV_{b} + EV_{s} + F.$$
(49)

We can find an explicit form for the different coefficients in this equation:

- $A = \frac{\partial C_{bb}}{\partial x}$  is related to the force of the bias electrode on charges polarized by its own potential. It can only vary over time due to changes in the geometry (or material properties) of the system.
- $B = 2\sum_{i=1}^{4} \frac{\partial C_{bs_i}}{\partial x}$  is related to the force that the signal electrodes exert on charges polarized by the bias electrode and vice-versa. It depends directly only in the geometry of the system.
- $C = \sum_{i=i}^{4} \sum_{j=1}^{4} \frac{\partial C_{s_i s_j}}{\partial x}$  is related to the force of all of the signal electrodes on all of the charges that each one and the others polarize when driven in unison. Same as A and B, it depends only on the geometry of the system.
- $D = -\left(\int_{\mathcal{V}} \left(\nabla \vec{f}_b \cdot \hat{e}_k\right) \rho_o(\vec{r'}) \mathrm{d}^3 \vec{r'} + \int_{\mathcal{V}} \rho_{\mathrm{free}}(\vec{r'}) \frac{\partial f_b(r')}{\partial r_k} \mathrm{d}^3 \vec{r'}\right) + 2 \frac{\partial \vec{C}_{b\vec{\Phi}}}{\partial x} \cdot \vec{\Phi}$ . Where  $\vec{C}_{b\vec{\Phi}}$  is the quadrant of the capacitance matrix relating the bias electrode and the potentials  $\vec{\Phi}$  considered irrelevant for actuation. It represents the forces between the bias electrode and charges induced in the object due to any other sources different than the bias or signal electrodes. This term can vary due to changes in the geometry of the system, due to changes in the potentials  $\vec{\Phi}$  or due to changes in the free charge distribution of the electrostatic array.
- $E = \sum_{i=1}^{4} \left[ -\left( \int_{\mathcal{V}} \left( \nabla \vec{f}_{s_i} \cdot \hat{e}_k \right) \rho_o(\vec{r'}) \mathrm{d}^3 \vec{r'} + \int_{\mathcal{V}} \rho_{\mathrm{free}}(\vec{r'}) \frac{\partial f_{s_i}(r')}{\partial r_k} \mathrm{d}^3 \vec{r'} \right) + 2 \frac{\partial \vec{C}_{s_i} \vec{\Phi}}{\partial x} \cdot \vec{\Phi} \right]$ . Where  $\vec{C}_{s_i} \vec{\Phi}$  is the quadrant of the capacitance matrix relating the signal electrode  $s_i$  and the potentials  $\vec{\Phi}$  considered irrelevant for actuation. It represents the forces between the signal electrodes (driven in unison) and charges induced in the object due to any other sources different than the bias or signal electrodes. This term can vary due to changes in the geometry of the system, due to changes in the potentials  $\vec{\Phi}$  or due to changes in the free charge distribution of the electrostatic array.
- $F = \vec{\Phi}^{\top} \frac{\partial \mathbf{C}_{\vec{\Phi}\vec{\Phi}}}{\partial r_k} \vec{\Phi} \left( \int_{\mathcal{V}} \left( \nabla \vec{f}_{\vec{\Phi}} \cdot \hat{e}_k \right) \rho_o(\vec{r'}) \mathrm{d}^3 \vec{r'} + \int_{\mathcal{V}} \rho_{\mathrm{free}}(\vec{r'}) \frac{\partial \vec{f}_{\vec{\Phi}}(\vec{r'})}{\partial r_k} \mathrm{d}^3 \vec{r'} \right) \cdot \vec{\Phi} + F_0$ . Where  $\mathbf{C}_{\vec{\Phi}\vec{\Phi}}$  is the quadrant of the capacitance matrix related to the potentials  $\vec{\Phi}$  and  $\vec{f}_{\vec{\Phi}}$  is a list of geometric potentials associated with the potentials  $\vec{\Phi}$ . It represents all of the electrostatic forces that are independent on  $V_b$  and  $V_s$ . This term can vary due to changes in the geometry of the system, due to changes on the potentials  $\vec{\Phi}$  or due to changes in the free charge distribution on the electrostatic array.

<sup>&</sup>lt;sup>34</sup> The list of potentials in  $\vec{\Phi}$  includes the suspension cage, ring heater, etc.

We can compare the first principles model from equation (49) to the semi-empirical model (15) used in [33]. The main difference between the two lies on the fact that the coefficients related to  $V_b^2$  and  $V_s^2$  (A and C, respectively) are equal in the case of the Advanced LIGO ESDs, since the geometry of the electrodes is virtually the same, and hence their interaction with the charges they polarize is the same [30]. On the other hand, the symmetry of the electrodes can be broken by asymmetric free charge accumulation (which affects terms D and E in equation (49)). This exercise then can help explain the possible origins for the time variation of the coefficients in (15).

#### Appendix D. Full derivation

The objective of this appendix is to formulate the more general versions of the electromechanical equations of motion (2) and (4) in order to include several moving objects as well as the possibility of rotations as well as translations.

#### D.1. General problem statement

Our system consists of N conductors C, linear dielectrics D and free charge distributions  $\rho_{\text{free}}$ . Everything under consideration is surrounded by an external conductor  $C_{N+1}$  which serves as the reference for all potentials (ground in the circuits). The mechanical part of this system is comprised by a subset of the system of conductors, dielectrics and free charges that can move as rigid bodies.<sup>35</sup> Each subset that acts as a rigid body will be called an 'object', the set of all objects being denoted by O.

For our treatment we assume that the conductors and dielectrics in the system have a very short relaxation time compared to the timescales of interest. On the other hand, we assume all insulators have a conductivity such that the reorganization of free charges inside them is many orders of magnitude longer than the timescales of relevance. We include the extra condition that magnetic fields are not relevant to our calculations. Under these assumptions we can treat the fields as quasi-static [16], meaning that the system can be described by an electromagnetic equilibrium state at all times.<sup>36</sup>. Since we disregard magnetic effects, the quasi-static electric field in the array can be described as the gradient of a scalar potential  $\phi$ .

In turn, the linearity of Maxwell's equations imply that given the position of all objects, the state of the system can be fully described by the potentials  $\vec{\phi} = \{\phi_i\}$  of each conductor, plus the values of the free charge density  $\rho_{\text{free}}$ . In turn, the charges  $\vec{q}$  of the conductors will be considered dependent variables.

Each conductor is connected through linear circuits to ideal voltage sources  $\vec{\phi}^{in}$ . In what follows, we assume that the potentials have only small variations around a set value, so that the equilibrium position of the system is well defined and time independent.

The positions of the objects are described in the way that is usual for rigid body mechanics [45]. Each object is represented by an instantaneous 'local' coordinate system located at the center of mass of each object. The position of object n is represented by the position  $\vec{r}_n$  of the origin of its coordinate systems relative to an overall, inertial coordinate frame.

 $<sup>^{35}</sup>$  For example, one can consider a dielectric mass with free charge embedded on it or a group of conducting plates attached to a dielectric.

<sup>&</sup>lt;sup>36</sup> Note that the timescale assumptions are essentially the same as the ones used to describe thermodynamic equilibrium states [25].

<sup>&</sup>lt;sup>37</sup> This is in contrast with the main body of the paper, where we decided to use subscripts to denote the coordinate directions.

Rotations of the objects are represented by changes in the orientation of the instantaneous coordinate system's axes. The angular position of object n is denoted by  $\vec{\theta}_n$ , which is used to represent the nautical angles (roll, pitch, yaw).

In what follows all variables are in the frequency domain to streamline the derivations.

#### D.2. Linearized equations

*D.2.1. Circuit equations.* Due to the linearity of the circuits we can change them to their Thévenin equivalents [22]. The circuit equations then are:

$$\frac{d\vec{q}}{dt} = \left(\mathbf{Z}^{\text{eq}}\right)^{-1} \left(\vec{\phi}^{\text{th}} - \vec{\phi}\right),\tag{50}$$

where  $\vec{\phi}_i^{\text{th}}$  represents the ideal potential sources of the of the Thévenin equivalent and  $Z_i^{\text{eq}}$  an equivalent impedance  $Z_i^{\text{eq}}$  Since we are treating  $\vec{q}$  as a dependent variable from the electrostatics of the problem (the potentials, positions and angles), we can write this as:

$$\mathbf{C}\frac{\mathrm{d}\vec{\phi}}{\mathrm{d}t} + \sum_{n} \left( \frac{\partial \vec{\mathbf{q}}}{\partial \vec{\mathbf{r}}_{n}} \frac{\mathrm{d}\vec{r}_{n}}{\mathrm{d}t} + \frac{\partial \vec{\mathbf{q}}}{\partial \vec{\Theta}_{n}} \frac{\mathrm{d}\vec{\theta}_{n}}{\mathrm{d}t} \right) = \left( \mathbf{Z}^{\mathrm{eq}} \right)^{-1} \left( \vec{\phi}^{\mathrm{th}} - \vec{\phi} \right), \tag{51}$$

where we used a short notation for the capacitance coefficients of the system. Under small oscillations, and keeping only terms of first order, the linearized circuit equations can be written in the frequency domain as:

$$((\mathbf{Z}^{\mathrm{eq}})^{-1} + i\omega\mathbf{C}_{\mathbf{0}})\delta\vec{\phi} + i\omega\sum_{n}\left(\left(\frac{\partial\vec{\mathbf{q}}}{\partial\vec{\mathbf{r}}_{n}}\right)_{0}\delta\vec{r}_{n} + \left(\frac{\partial\vec{\mathbf{q}}}{\partial\vec{\mathbf{\Theta}}_{n}}\right)_{0}\delta\vec{\theta}_{n}\right) = \left(\mathbf{Z}^{\mathrm{eq}}\right)^{-1}\delta\vec{\phi}^{\mathrm{th}}.$$
 (52)

The right-hand side of this equation has the contribution from the (small) oscillating drive signal through  $\vec{\phi}^{\text{th}}$ . We also can recognize the matrix on the left-hand side of equation (52) to be the conductance matrix **G** [22] of the equivalent circuit<sup>38</sup> for the electrical part of the system.<sup>39</sup>

*D.2.2. Mechanical equations.* Since we are observing the center of mass of each object, the translational component of the equations of motion reduce simply to the common expression for Newton's second law:

$$\mathbf{M}_{n} \frac{\mathrm{d}^{2} \vec{r}_{n}}{\mathrm{d}t^{2}} = \vec{F}_{n},\tag{53}$$

where  $\vec{F}_n$  are the external forces acting on object n and  $\mathbf{M}_n$  is a diagonal matrix with the mass of object n in each nonzero entry.

Under small oscillations around an equilibrium position, this can be recast as:

$$-\omega^{2}\mathbf{M}_{n}\delta\vec{r}_{n} = \sum_{m} \left( \mathbf{K}_{(nm)}\delta\vec{r}_{m} + \left( \frac{\partial\vec{\mathbf{F}}_{n}}{\partial\vec{\boldsymbol{\Theta}}_{m}} \right)_{0}\delta\vec{\theta}_{m} \right) + \left( \frac{\partial\vec{\mathbf{F}}_{n}}{\partial\vec{\boldsymbol{\Phi}}} \right)_{0}\delta\vec{\phi}, \tag{54}$$

where the stiffness matrix  $\mathbf{K}_{(nm)}$  are  $3 \times 3$  matrices which connect the displacement of object m with the mechanical force on object n. Specifically, the entry ij of  $\mathbf{K}_{(nm)}$  connects the force

 $<sup>^{38}</sup>$  The equivalent circuit can be written by changing the conductors by conductor nodes and the capacitance matrix by a network of mutual capacitances  $\mathbf{C}^{m}$  [46].

<sup>&</sup>lt;sup>39</sup> The conductance matrix approach can be used to generalize these equations for situations where there are impedances connecting the different connectors. For simplicity we will not focus on those examples on this derivation.

object n feels in the direction i due to movements of object m in direction j. The coupling to the angular degrees of freedom, as well as the electromechanical coefficients are left as partial derivatives.

The evolution of the rotational degrees of freedom are given by the general equation:

$$\mathbf{I}_{n} \frac{d\vec{\Omega}_{n}}{dt} + \vec{\Omega}_{n} \times \left(\mathbf{I}_{n} \vec{\Omega}_{n}\right) = \vec{\tau}_{n},\tag{55}$$

where  $\Omega_n$  represents the instantaneous angular velocity vector of the body. The torques and inertia tensors are understood to be seen from the center of mass frame of each object. If we choose the 'nautical' convention for the Euler angles  $\vec{\theta_n}^{40}$  and set  $\vec{\theta_n} = 0$  for the equilibrium position, then  $\delta \vec{\Omega}_n = \frac{\mathrm{d}}{\mathrm{d}t} \delta \vec{\theta}_n$  for small perturbations. With this definition, equation (55) reduces to:

$$-\omega^{2}\mathbf{I}_{n}\delta\vec{\theta}_{n} = \sum_{m} \left(\mathbf{K}_{(nm)}^{\theta}\delta\vec{\theta}_{m} + \left(\frac{\partial\vec{\tau}_{n}}{\partial\vec{\mathbf{r}}_{m}}\right)_{0}\delta\vec{r}_{m}\right) + \left(\frac{\partial\vec{\tau}_{n}}{\partial\vec{\Phi}}\right)_{0}\delta\vec{\phi}.$$
 (56)

Similar to the translation equation, we have written the rotational stiffness between two different objects as  $\mathbf{K}_{(nm)}^{\theta}$ .

#### D.3. Johnson noise

Equations (52), (54) and (56) represent the linearized equations of motion. The Johnson noise contribution can be accounted for by adding N independent white current noise sources  $|\eta_i|^2 = 4k_bT \operatorname{Re}(1/Z_i^{\text{eq}})$  to each subcircuit. The superposition principle implies that we can treat the source terms  $\delta \phi^{\text{th}}$  as zero for this analysis.

The resulting effect on the mechanical variables can be computed by solving for  $\delta \vec{\phi}$  in the circuit equation (52) and plugging it into the different mechanical equations to obtain:

$$-\omega^{2}\mathbf{M}_{n}\delta\vec{r}_{n} = \sum_{m\in\mathcal{O}}\left[\mathbf{K}_{nm}\delta\vec{r}_{m} + \left(\frac{\partial\vec{\mathbf{F}}_{n}}{\partial\vec{\mathbf{\Theta}}_{m}}\right)_{0}\delta\vec{\theta}_{m} + i\omega\left(\frac{\partial\vec{\mathbf{F}}_{n}}{\partial\vec{\mathbf{\Phi}}}\right)_{0}\mathbf{G}^{-1}\left(\left(\frac{\partial\vec{\mathbf{q}}}{\partial\vec{\mathbf{r}}_{m}}\right)_{0}\delta\vec{r}_{m} + \left(\frac{\partial\vec{\mathbf{q}}}{\partial\vec{\mathbf{\Theta}}_{m}}\right)_{0}\delta\vec{\theta}_{m}\right)\right] + \vec{F}_{n}(\vec{\eta}),$$
(57)

$$-\omega^{2} \mathbf{I}_{n} \delta \vec{\theta}_{n} = \sum_{m \in \mathcal{O}} \left[ \mathbf{K}_{nm}^{\theta} \delta \vec{\theta}_{m} + \left( \frac{\partial \vec{\mathbf{r}}_{n}}{\partial \vec{\mathbf{r}}_{m}} \right)_{0} \delta \vec{r}_{m} + i\omega \left( \frac{\partial \vec{\mathbf{r}}_{n}}{\partial \vec{\mathbf{\Phi}}} \right)_{0} \mathbf{G}^{-1} \left( \left( \frac{\partial \vec{\mathbf{q}}}{\partial \vec{\mathbf{r}}_{m}} \right)_{0} \delta \vec{r}_{m} + \left( \frac{\partial \vec{\mathbf{q}}}{\partial \vec{\mathbf{\Theta}}_{m}} \right)_{0} \delta \vec{\theta}_{m} \right) \right] + \vec{\tau}_{n}(\vec{\eta}). \quad (58)$$

The forces and torques induced by the Johnson noise are given by:

$$\vec{F}_n(\vec{\eta}) = \left(\frac{\partial \vec{\mathbf{F}}_n}{\partial \vec{\boldsymbol{\Phi}}}\right)_0 \mathbf{G}^{-1} \vec{\eta} \quad ; \quad \vec{\tau}_n(\vec{\eta}) = \left(\frac{\partial \vec{\boldsymbol{\tau}}_n}{\partial \vec{\boldsymbol{\Phi}}}\right)_0 \mathbf{G}^{-1} \vec{\eta}. \tag{59}$$

The total Johnson noise contribution to the different degrees of freedom can be calculated by adding the contributions of each independent noise source  $\eta_i$  in quadrature.

<sup>&</sup>lt;sup>40</sup> This refers to the convention in which each angle represents a rotation along a different local axis.

#### D.4. Approximate forms

The general form of these equations is complicated and it involves solving for the resonances of the system. However, if we assume that our frequencies of interest are such that we can consider the system to be inertial, then the force and torque equations simplify to:

$$-\omega^2 \mathbf{M}_n \delta \vec{r}_n = \left(\frac{\partial \vec{\mathbf{F}}_n}{\partial \vec{\Phi}}\right)_0 \mathbf{G}^{-1} \vec{\eta},\tag{60}$$

$$-\omega^2 \mathbf{I}_n \delta \vec{\theta}_n = \left(\frac{\partial \vec{\tau}_n}{\partial \vec{\Phi}}\right)_0 \mathbf{G}^{-1} \vec{\eta}. \tag{61}$$

Moreover, if we assume that  $G \approx (\mathbf{Z}^{eq})^{-1}$  (meaning that the conductance contributed by the capacitance matrix can be considered to be zero at the frequencies of interest), then we obtain the more familiar forms:

$$-\omega^2 \mathbf{M}_n \delta \vec{r}_n = \left(\frac{\partial \vec{\mathbf{F}}_n}{\partial \vec{\mathbf{\Phi}}}\right)_0 \mathbf{Z}^{\text{eq}} \vec{\eta},\tag{62}$$

$$-\omega^2 \mathbf{I}_n \delta \vec{\theta}_n = \left(\frac{\partial \vec{\tau}_n}{\partial \vec{\Phi}}\right)_0 \mathbf{Z}^{\text{eq}} \vec{\eta}. \tag{63}$$

Then, for the translation of a given object in the x direction, due to a single noise source  $\eta_i$  we find:

$$\delta x_n = \frac{-1}{m_n \omega^2} \left( \frac{\partial F_{n,x}}{\partial \phi_i} \right) Z_i^{\text{eq}} \eta_i \implies |\delta x_n|^2 = \frac{1}{(m_n \omega^2)^2} \left( \frac{\partial F_{n,x}}{\partial \phi_i} \right)^2 4k_b T \operatorname{Re} \left( Z_i^{\text{eq}} \right),$$
(64)

where we have used Re  $\left(\frac{1}{z}\right) = \frac{\text{Re}(z)}{|z|^2}$  for complex numbers z. Adding the noise sources in quadrature yields:

$$|\delta x_n| = \frac{\sqrt{4k_b T}}{m_n \omega^2} \sqrt{\sum_{i \in \mathcal{C}} \left(\frac{\partial F_{n,x}}{\partial \phi_i}\right)_0^2 \operatorname{Re}(Z_i^{\text{eq}})},\tag{65}$$

which is equivalent to the form (12) given in the main paper.

#### **ORCID iDs**

Edgard Bonilla https://orcid.org/0000-0002-6284-9769 Brian Lantz https://orcid.org/0000-0002-7404-4845 Aaron Buikema https://orcid.org/0000-0001-9409-5757

#### References

- [1] Abbott B P *et al* 2016 Observation of gravitational waves from a binary black hole merger *Phys. Rev. Lett.* **116** 061102
- [2] Abbott B P et al 2019 GWTC-1: a gravitational-wave transient catalog of compact binary mergers observed by LIGO and Virgo during the first and second observing runs *Phys. Rev.* X **9** 031040

- [3] LIGO Scientific Collaboration 2020 GWTC-2: compact binary coalescences observed by LIGO and Virgo during the first half of the third observing run LIGO Document:LIGO-P2000061 (in preparation)
- [4] Abbott B P et al 2017 Multi-messenger observations of a binary neutron star merger Astrophys. J. Lett. 848 L12
- [5] LIGO Scientific Collaboration, Virgo Collaboration, 1M2H Collaboration, Dark Energy Camera GW-EM Collaboration, DES Collaboration, DLT40 Collaboration, Las Cumbres Observatory Collaboration, VINROUGE Collaboration, MASTER Collaboration et al 2017 A gravitationalwave standard siren measurement of the Hubble constant Nature 551 85–8
- [6] Abbott B P et al 2018 GW170817: measurements of neutron star radii and equation of state Phys. Rev. Lett. 121 161101
- [7] Abbott B P et al 2019 Binary black hole population properties inferred from the first and second observing runs of Advanced LIGO and Advanced Virgo Astrophys. J. Lett. 882 L24
- [8] LIGO Scientific Collaboration and Virgo Collaboration 2020 GraceDB—O3 gravitational-wave candidate database https://gracedb.ligo.org/superevents/public/O3/
- [9] Martynov D V et al 2016 Sensitivity of the Advanced LIGO detectors at the beginning of gravitational wave astronomy Phys. Rev. D 93 112004
- [10] Buikema A et al 2020 Sensitivity and performance of the Advanced LIGO detectors in the third observing run Phys. Rev. D 102 062003
- [11] Frolov V 2019 Comment on BNS range vs power projection Technical Report LIGO Livingston Observatory log 45943
- [12] Kissel J and Prokhorov L 2016 Interaction of the ESD with electrical charges of the test masses in Advanced LIGO LIGO Document: LIGO-G1600699
- [13] Rollins J and Smith N 2014 Thermal noise of an electromechanical pendulum Technical Report LIGO Livingston Observatory log 14566
- [14] Lantz B 2014 Estimate of force coupling between charged optic face and optic cage LIGO Document:LIGO-G1401179
- [15] Haus H A and Melcher J R 1989 Electromagnetic Fields and Energy vol 107 (Englewood Cliffs, NJ: Prentice-Hall)
- [16] Landau L D, Bell J S, Kearsley M J, Pitaevskii L P, Lifshitz E M and Sykes J B 2013 Electrodynamics of Continuous Media vol 8 (Amsterdam: Elsevier)
- [17] Harry G M *et al* 2006 Titania-doped tantala/silica coatings for gravitational-wave detection *Class. Quantum Grav.* **24** 405
- [18] Cagnoli S M et al 2012 Update on quadruple suspension design for Advanced LIGO Class. Quantum Grav. 29 235004
- [19] Cunningham A F et al 2016 Overview of Advanced LIGO adaptive optics Appl. Opt. 55 8256-65
- [20] LIGO Scientific Collaboration 2015 Instrument Science White paper. LIGO Document:LIGO-T1400316
- [21] Jacobson R and Fritschel P 2015 ETM Low Voltage Low Noise Electro-Static Driver Main Board LIGO Document LIGO-D1500016
- [22] Alexander C K and Sadiku M N O 2000 Fundamentals of Electric circuits (New York: McGraw-Hill)
- [23] Griffiths D J 2013 Introduction to Electrodynamics (Boston, MA: Pearson Education Inc.)
- [24] Di Lorenzo E 2011 The Maxwell Capacitance Matrix FastFieldSolvers White Paper: WP110301
- [25] Reif F 2009 Fundamentals of Statistical and Thermal Physics (Long Grove, IL: Waveland Press)
- [26] Callen H B and Welton T A 1951 Irreversibility and generalized noise *Phys. Rev.* 83 34
- [27] Callen H B and Greene R F 1952 On a theorem of irreversible thermodynamics *Phys. Rev.* **86** 702
- [28] Van Kampen N G 1992 Stochastic Processes in Physics and Chemistry vol 1 (Amsterdam: Elsevier)
- [29] Kubo R 1966 The fluctuation-dissipation theorem Rep. Prog. Phys. 29 255
- [30] Buikema A 2020 PhD Thesis Massachusetts Institute of Technology
- [31] Aston S 2020 Running full in-lock charge measurement for ETMX Technical Report LIGO Livingston Observatory log 51289
- [32] Aston S 2020 Running full in-lock charge measurement for ETMY Technical Report LIGO Livingston Observatory log 51286
- [33] Dwyer S, Kissel J and Mavalvala N 2017 ESD actuation strength measurements LIGO Document:LIGO-T1700446
- [34] Aasi J et al (Advanced LIGO) 2015 Class. Quantum Grav. 32 074001

- [35] Buikema A 2019 In-lock charge measurement trends Technical Report LIGO Livingston Observatory log 43493
- [36] Blair C et al 2017 First demonstration of electrostatic damping of parametric instability at Advanced LIGO Phys. Rev. Lett. 118 151102
- [37] Barsotti L, Fritschel P, Evans M and Gras S 2018 Updated Advanced LIGO sensitivity design curve LIGO Document:LIGO-T1800044
- [38] Kissel J et al 2015 Updated Advanced LIGO sensitivity design curve LIGO Document:LIGO-G1500623
- [39] Adhikari R X et al 2020 A cryogenic silicon interferometer for gravitational-wave detection (arXiv:2001.11173)
- [40] Punturo M et al 2010 The Einstein Telescope: a third-generation gravitational wave observatory Class. Quantum Grav. 27 194002
- [41] Komori K, Enomoto Y, Takeda H, Michimura Y, Somiya K, Ando M and Ballmer S W 2018 Direct approach for the fluctuation—dissipation theorem under nonequilibrium steady-state conditions *Phys. Rev.* D 97 102001
- [42] Auslender M and Hava S 2017 Single-Crystal Silicon: Electrical and Optical Properties (Berlin: Springer) p 1
- [43] Panofsky W K H and Phillips M 2005 Classical Electricity and magnetism (New York: Dover)
- [44] Herrera W J and Diaz R A 2008 The geometrical nature and some properties of the capacitance coefficients based on Laplace's equation *Am. J. Phys.* **76** 55–9
- [45] Goldstein H, Poole C and Safko J 2002 Classical Mechanics (Boston, MA: Pearson Education Inc.)
- [46] Tausch J and White J 1999 Capacitance extraction of 3D conductor systems in dielectric media with high-permittivity ratios IEEE Trans. Microw. Theory Tech. 47 18–26